Fault growth at a nascent slow-spreading ridge: 2005 Dabbahu rifting episode, Afar

J. V. Rowland,[1] E. Baker,[2] C. J. Ebinger,[3] D. Keir,[2] T. Kidane,[4] J. Biggs,[5] N. Hayward[6] and T. J. Wright[7]

[1] *School of Geography, Geology and Environmental Science, University of Auckland, New Zealand. E-mail: j.rowland@auckland.ac.nz*
[2] *Department of Geology, Royal Holloway University of London, United Kingdom*
[3] *Earth & Environmental Sciences, University of Rochester, USA*
[4] *Department of Earth Science, Addis Ababa University, Ethiopia*
[5] *Centre for the Observation and Modelling of Earthquakes and Tectonics, Department of Earth Sciences, University of Oxford, United Kingdom*
[6] *Talisman Energy (UK) Ltd.*
[7] *School of Earth & Environment, University of Leeds, United Kingdom*

SUMMARY

We present a preliminary account of the near-field surface strain associated with a major magmatic rifting episode at a nascent slow spreading ridge in the Afar depression. Between 2005 September 14 and October 4, a volcanic eruption and 163 earthquakes ($m_b > 3.9$), including seismic tremor, occurred within the ∼60-km-long Dabbahu magmatic segment. Results of the early response team demonstrated that ground deformation, derived from satellite radar data (InSAR), together with seismicity, is consistent with dyke-induced deformation along the entire length of the segment. We document the distribution of brittle strain associated with the early part of this rifting cycle to verify the predicted pattern of deformation and constrain a conceptual model for normal fault growth in Afar, with general application to other slow spreading divergent margins. Our field investigations concentrate on the northern half of the segment, which ruptured through to the surface over a length of >30 km and a width of ∼5 km, consistent with the pattern of microseismicity recorded using a network deployed ∼1 month after the initial onset of the rifting episode on September 14. Severe ground shaking during the event was more widespread; fresh rock fall is common across the entire magmatic segment, particularly at the intersections between faults. Recent ground breaks, in the form of reactivated or newly initiated normal faults and fissures, opened with horizontal displacements up to 3 m and vertical displacements locally up to 5 m, but commonly ∼2 m. These structures are generally subvertical and open along pre-existing cooling joints. Fault offset is greater than expected given the magnitude of earthquakes during the episode. The axial relief that developed consequent on fault and fissure initiation and reactivation during the 2005 Dabbahu episode is consistent with that of the entire magmatic segment. We therefore suggest that melt delivery is sufficiently frequent that favourable stress conditions for faulting are primarily achieved during dyke events.

Key words: continental margins, extension, normal faulting, rifts.

1 INTRODUCTION

Crustal growth at divergent plate boundaries develops as a consequence of dyke intrusion. The passage of these intrusions is recorded in the sheeted dyke complex of oceanic crustal layer 2B, which demonstrates that dykes efficiently accommodate most of the plate separation at oceanic ridges. Dyke intrusion also appears to be important within rifts transitional from continental to oceanic, where dykes accommodate an equal or possibly larger proportion of strain than recent normal faults (Klausen & Larsen 2002; Bendick *et al.*

2006; Keir *et al.* 2006a). An instantaneous and localized extension accompanies dyke intrusion and is marked by shallow, small magnitude and sometimes long-period earthquake swarms, with or without surface breaks and effusive volcanism. These dyke events may occur singly or as a succession of discrete intrusions over several years, followed by a decadal-scale relaxation transient that is larger than the time-averaged plate divergence (e.g. Heki *et al.* 1993). The periodic repetition of this process is recorded in the morphology as individual tectono-magmatic segments and over time leads to opening rates consistent with far-field plate motions. Beyond these

simple concepts, there is no consensus on what controls the rifting cycle and still very little information on how strain is distributed, in space and time, at divergent plate boundaries.

To a first order, oceanic ridge segment morphology appears to vary quasi-systematically with geological and geophysical indicators of magmatism (e.g. Langmuir *et al.* 1986; Macdonald *et al.* 1988; Kent *et al.* 2000; Van Adendonk *et al.* 2001), such that shallow broad ridges are believed to reflect enhanced magma supply, and deeper, more tectonized segments are assumed to be magma-starved. Such a scheme provides a satisfactory explanation for the difference in morphology between fast spreading ridges with high melt flux and intermediate and slow spreading ridges, where the supply of melt from the mantle is viewed as spatially variable and time-dependent (e.g. Lin & Phipps Morgan 1992; Dick *et al.* 2003). However, because dyke intrusion can accommodate the far-field pull of plate tectonics at lower stress than is required for fault slip (e.g. Parsons *et al.* 1998), many authors assume that plate spreading is partitioned between tectonic faulting and magmatism such that faults form only where or when melt supply is reduced (Tucholke & Lin 1994; Thatcher & Hill 1995; Dunn *et al.* 2005; Pierce *et al.* 2005). Geometrical analyses of faults and fissures, and interpretations of fault strain from topographic and bathymetric data, have been used to quantify deformation partitioning in active rifts. Extensional normal faults accommodate 5–10 per cent of the total spreading rate along the East Pacific Rise (Cowie *et al.* 1993), 5–15 per cent of the total extension in the Asal Rift, Djibouti (De Chabalier & Avouac 1994) and 50 per cent of the extension in the northern Krafla rift, Iceland (Dauteuil *et al.* 2001). However, since the distribution of brittle strain associated with dyke events is unknown, caution is required when using these estimates to infer ratios of tectonism to magmatism. Theoretical arguments and sparse real-time observations demonstrate that normal fault growth and related subsidence may occur in tandem with dyke intrusion (Brandsdóttir & Einarsson 1979; Rubin 1992). This raises the possibility that a component of fault slip in these studies and at other slow and intermediate spreading ridges is consequent on repeated cycles of magmatism (e.g. Carbotte *et al.* 2006; Singh *et al.* 2006).

These competing models highlight the need to quantify how strain is distributed in space and time at divergent plate boundaries. The actual process of dyke intrusion is rarely recorded and yet to be observed directly in submarine settings. We therefore rely on observations of strain accommodation and magma cycling from a few subaerial rift zones to test the basic models of seafloor spreading processes (e.g. Fox *et al.* 1995). The subaerial rift zones in Iceland and Djibouti afford vital glimpses of dyke injection processes at divergent plate boundaries. The 2-month long 1978 Asal-Ghoubbet event, Djibouti, commenced with an $m_b = 5.3$ event near the centre of a 60 km-long segment followed by a week-long volcanic eruption (e.g. Abdallah *et al.* 1979). Cattin *et al.* (2005) interpret the spatial and temporal pattern of deformation as being associated with a 5 yr-long dyke intrusion episode. From 1975 to 1984, 20 dykes were intruded during the Krafla rifting episode, which developed along a pre-existing, 70-km-long segment of the Northern Rift Zone in Iceland (e.g. Bjornsson *et al.* 1977; Einarsson 1991; Sigmundsson 2006). Dykes were fed from the Krafla magma chamber near the centre of the segment and most dykes intruded along new and existing fissures in a <2-km-wide zone. Geodetic models reveal a significant longer term opening (Foulger *et al.* 1992) indicative of an additional deeper source modelled at the base of the crust (de Zeeuw-van Dalfsen *et al.* 2004). Slip was ≤2 m in the first, largely intrusive event, which was characterized by earthquakes as deep as 10 km (Einarsson & Brandsdóttir 1980). Successive dyking events propagated shorter distances along the rift and the last few events were more effusive. The distribution of intrusive events and the segment-scale pattern of surface deformation at Krafla demonstrate the importance of dyke intrusion to the creation and maintenance of the regular along-axis segmentation characteristic of such rifts.

From 2005 September 14 to October 4, a tectono-magmatic episode of unprecedented scale and intensity occurred along a previously defined segment of the Afar rift, Ethiopia (Fig. 1). The brief event consisted of a 60-km-long dyke intrusion, 163 earthquakes (5.6 > m_b > 3.9), and the emplacement of ~2.5 km³ of magma (Wright *et al.* 2006; Ayele *et al.* 2007). This is the largest single magmatic rifting episode known to have occurred on land since the
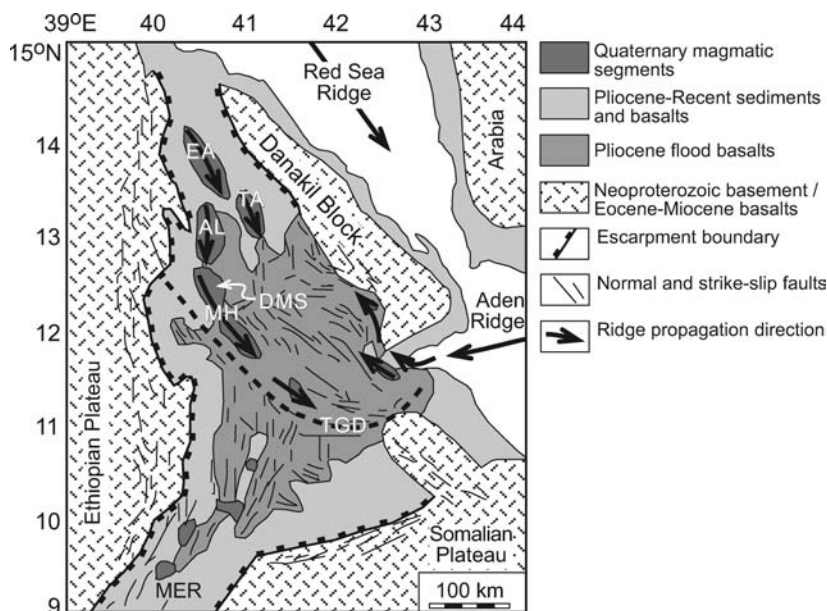

Figure 1. Geological map of the Afar Depression, after Barberi & Varet (1977) and Hayward & Ebinger (1996) showing the distribution of subaerial Quaternary magmatic segments. EA = Erta'Ale, TA = Tat'Ale, AL = Alayta, MH = Manda-Hararo. A rifting episode initiated within the Dabbahu Magmatic Segment (DMS) on 2005 September 14. TGD = Tendaho Gobaad Discontinuity (thick dashed line) and MER = Main Ethiopian Rift.

Laki (Iceland) eruption in 1783, and the first in the era of satellite geodesy. The early geodetic, seismic and volcanological response to the episode has ensured a nearly continuous record of events from onset of the rifting cycle (see Ebinger *et al.* 2006; Wright *et al.* 2006; Yirgu *et al.* 2006; Ayele *et al.* 2007).

In this paper, we provide a preliminary account of the distribution of brittle strain associated with the early part of the 2005 Afar rifting cycle to: (1) verify the pattern of deformation predicted in 3-D models derived from satellite radar data; (2) highlight the scale of fault growth associated with the initial period of dyke intrusion before the newly formed structures are obscured by late stage extrusive lavas and (3) compare qualitatively with the finite strain recorded in the morphology of the entire segment. A conceptual model is then developed for normal fault growth in Afar with general application to the evolution of tectono-magmatic segments at slow spreading divergent margins. Quantitative strain analyses and fault scaling relationships will be provided in a later publication once suitable topographic imagery (LiDAR) has been acquired and further field work has been undertaken.

2 TECTONIC SETTING

Rifting between Africa and Arabia during the past ∼30 Myr produced the ∼300-km-wide Afar depression at the triple junction between the Red Sea, Gulf of Aden, and East African rifts (Fig. 1). These extensional provinces formed within a Palaeogene flood basalt province associated with the Afar mantle plume (e.g. Schilling *et al.* 1992; Hofman *et al.* 1997). The thermal anomaly associated with this plume persists today, as shown by low *P-* and *S*-wave upper-mantle velocities beneath the uplifted plateaus of Arabia and NE Africa (Benoit *et al.* 2003; Montelli *et al.* 2004; Bastow *et al.* 2005; Benoit *et al.* 2006). Rifting within the Red Sea and Gulf of Aden arms of the triple junction has progressed to oceanic spreading (e.g. Manighetti *et al.*1998), whereas the less-evolved Main Ethiopian Rift (MER) is transitional from continental rifting to oceanic seafloor spreading (Hayward & Ebinger 1996). The crust of the Afar depression is highly extended and intruded with high Vp/Vs indicating a mafic composition (Dugda & Nyblade 2006). Crustal thickness ranges from 18 km in the north to 24 km in the south (Berckhemer *et al.* 1975; Tiberi *et al.* 2005; Stuart *et al.* 2006). Many authors have used topographic and palaeomagnetic data to investigate rift evolution, ridge propagation and normal fault growth within the Afar depression (e.g. Courtillot *et al.* 1984; Tapponier *et al.* 1990; Acton *et al.* 2000; Gupta & Scholz 2000; Manighetti *et al.* 2001; Kidane *et al.* 2003; Lahitte *et al.* 2003). Notwithstanding these contributions, constraints on crustal structure are sparse. However, important insights as to the tectono-magmatic processes operating within the Afar depression may be extrapolated from recent investigations into the lithospheric structure of the MER. Currently, strain in the MER is localized within narrow zones of aligned eruptive magmatic centres and small displacement normal faults that developed ∼2 Ma within broad monoclinal basins bounded by high-angle border faults of Miocene age (Ebinger & Casey 2001). Seismic refraction and tomography models demonstrate that the mantle lithosphere is thin (<50 km) beneath the rift valley (Bastow *et al.* 2005), and up to 25 per cent of the crustal volume comprises intrusive or extrusive igneous rocks (Mackenzie *et al.* 2005). Dense, relatively high velocity crust underlies the magmatic segments and is interpreted as ∼10–15-km wide basaltic intrusions or dyke swarms (Keranen *et al.* 2004), sourced from the asthenosphere (Furman *et al.* 2006). Observations of shear wave splitting in the upper mantle and crust demonstrate that seismic anisotropy parallels the orientation of the magmatic segments, consistent with a melt-filled crack model (Keir *et al.* 2005; Kendall *et al.* 2005). Thus, within the MER, and presumably also within Afar, there has been a transition from extension via crustal-scale detachment faults to magma intrusion and minor faulting in the upper crust above magma injection zones.

Within the southern Red Sea Rift and Afar, the initial development of border faults was roughly coincident with the 31–29 Ma flood basalt sequences in the same area (Wolfenden *et al.* 2005). Strain migrated riftward from 19 to 12 Ma (Wolfenden *et al.* 2005), and by ∼5 Ma, an oceanic spreading ridge had developed within the south-central Red Sea rift (Cochran 1983). Southward propagation of the ridge isolated the Danakil block between a truly oceanic rift branch to the northeast and a subaerial rift zone to the southwest within the Afar depression. Since ∼3 Ma, faulting and volcanism within the subaerial southern Red Sea rift has localized to ∼60-km-long magmatic segments comprising aligned chains of basaltic cones, strato-volcanoes, shallow seismicity and positive gravity anomalies (Fig. 1) (Barberi & Varet 1977). Currently, the subaerial southern Red Sea rift is extending in a northeast direction at a rate of <20 mm yr^{-1} (Jestin *et al.* 1994; Chu & Gordon 1998; Vigny *et al.* 2006).

The boundary of each magmatic segment is defined by the limits of the Quaternary volcanic flows associated with it (Hayward & Ebinger 1996). Along-axis segment terminations are topographic lows where faults from adjacent segments curve towards each other. Of importance here, there are no orthogonal fault zones (*cf.* transform faults) linking adjacent segments (Hayward & Ebinger 1996). Rather, the distribution of faulting at segment terminations is consistent with the fracture patterns expected for interacting en echelon crack tips (e.g. Pollard & Aydin 1984) and kinematically analogous to non-transform offsets along slow spreading ridges (e.g. Sempéré *et al.* 1993).

The northernmost magmatic segments, Erta'Ale and Tat'Ale, are characterized by axial volcanic ridges (AVR) of transitional alkali/tholeitic composition (Barberi *et al.* 1972). These AVRs extend the length of their respective segments, are elevated topographically (<700 m high), and are cut by numerous small, closely spaced normal faults and fissures that are parallel to, and decrease in age towards, the AVR axes. Sparse K-Ar data for basaltic and silicic rocks sampled within this sector of the subaerial Red Sea Rift indicate an age range of 1.46–0.52 Ma (Lahitte *et al.* 2003). Southward continuation of the Red Sea rift steps to the west along the Alayta magmatic segment and the Manda-Hararo rift zone (Fig. 1). The latter comprises the active Dabbahu segment, which is described in this paper, and the adjacent but currently quiet Hararo segment. In contrast to the broad highs that are common to magmatic segments of northern Afar, the morphology of the Manda-Hararo rift zone is characterized by a 35-km-wide central depression, which is punctuated by silicic edifices (Lahitte *et al.* 2003). Nonetheless, the prevalence of recent basaltic fissural flows along the axial zone demonstrates that the Manda-Hararo rift zone is the current locus of magmatism. These active magmatic segments are similar in scale and structural morphology to second-order slow-spreading oceanic ridge segments (Hayward & Ebinger 1996; Oppenheimer & Francis 1997). Abandoned magmatic segments of similar morphology lie between the Western Afar escarpment and the present locus of deformation, indicating that strain accommodation in narrow zones of magma injection is a ubiquitous part of the continental rupture process (Wolfenden *et al.* 2005).

In the following sections, we describe the structural architecture of the Dabbahu (also known as Boina or Boyna) segment, and

document the nature and distribution of brittle strain associated with the early part of the 2005 Dabbahu rifting episode.

3 DABBAHU MAGMATIC SEGMENT (DMS)

The Dabbahu magmatic segment (DMS) is ∼60 km in length and ∼15 km wide (Fig. 2). The orientation of the segment changes near Ado'Ale, a dissected, silicic central volcanic complex (Lahitte *et al.* 2003). In the vicinity and to the south of the Ado'Ale edifice the segment trends NW–SE, which is near orthogonal to the inferred extension direction (Jestin *et al*. 1994). To the north of Ado'Ale, the segment swings to a more northerly trend such that the rift axis is oriented c. 60° oblique to the direction of relative plate motion. Numerous active volcanoes occur at the northern tip of the segment, including the major silicic strato-volcano, Dabbahu, after which the magmatic segment is named, and the somewhat smaller Gab'ho volcano. Dabbahu volcano, standing 1350 m a.s.l. and with a diameter of ∼10 km, is the largest topographic load in the segment (Fig. 3). Gab'ho volcano reaches 850 m a.s.l. and is elliptical in plan view; major axes trend N–S and E–W, with lengths of 4.5 and 3 km, respectively. Smaller volcanoes and cinder cones define a linear vent zone to the northwest of Dabbahu volcano. Between Dabbahu volcano and Ado'Ale, the segment is elevated up to 150 m above the regional level of ∼400 m a.s.l. A well-developed axial graben extends from the southern flank of Dabbahu volcano to the south, but its topographic expression diminishes towards Ado'Ale, coextensive with a reduction in the general elevation of the segment (Fig. 4,

section E). Although heavily dissected, the Ado'Ale volcanic complex reaches elevations of >750 m a.s.l. and extends over a broad region of the central DMS. Ado'Ale constitutes a significant topographic load on the present tectono-magmatic system, and may have been an important influence on the current configuration of faulting (e.g. van Wyk de Vries & Merle 1996; Lahitte *et al.* 2003). South of Ado'Ale, the elevation of the rift zone is less than the regional level (Fig. 4, sections G–I).

Covering an area of nearly 2000 km², the DMS contains over 1200 distinct faults (Fig. 5), as recognized by Hayward (1997) from a quantitative analysis of rift architecture using ≤30 m resolution Landsat TM and <15 m resolution Large Format Camera space shuttle photography. Note that this resolution does not allow discrimination between faults in the strict sense (i.e. Coulomb shears), and faulted fissures (i.e. extensional shears), which from field inspection are the predominant mode of brittle failure. Faults have a mean strike of 333° (Fig. 5 inset), oblique to the NE-trending extension direction (Jestin *et al*. 1994; Vigny *et al.* 2006), but there is considerable variation. The greatest range in strike occurs just north of Ado'Ale, where the overall trend of the segment changes direction. South of Ado'Ale where rifting is orthogonal, the mean strike of faults is perpendicular to the extension direction. However, North of Ado'Ale where rifting is oblique, the mean strike of faults is 352°, parallel to the rift axis and oblique to the extension direction. Analogue models of orthogonal and oblique rifting demonstrate that rift basins are defined by segmented border fault systems that are parallel to the rift axes and by intrarift fault systems that are sub-perpendicular to the extension direction (e.g. McClay *et al*. 2002).
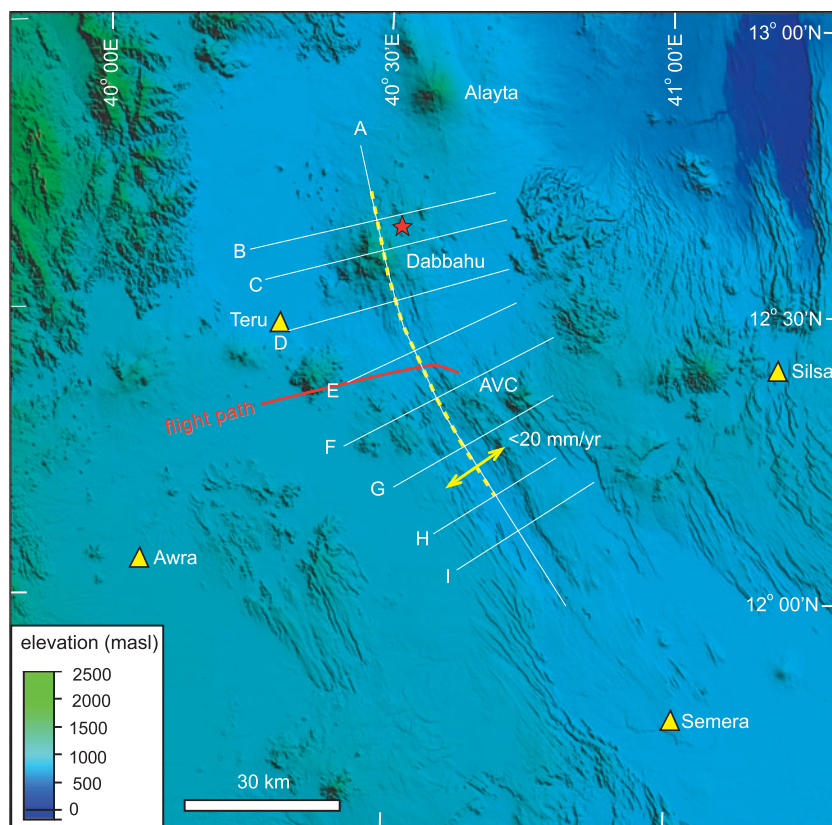

Figure 2. Digital elevation model of the Dabbahu magmatic segment showing location of the 2005 September 26 volcanic eruption (red star) within the Dabbahu volcanic edifice, AVC = Ado'Ale Volcanic Complex, villages (yellow triangles), the approximate position of the segment axis (dashed yellow line), the full extension direction and rate (Jestin *et al.* 1994), and the flight line (red) used to obtain the images shown in Fig. 6. Positions of topographic profiles (Figs 3 and 4) are indicated.
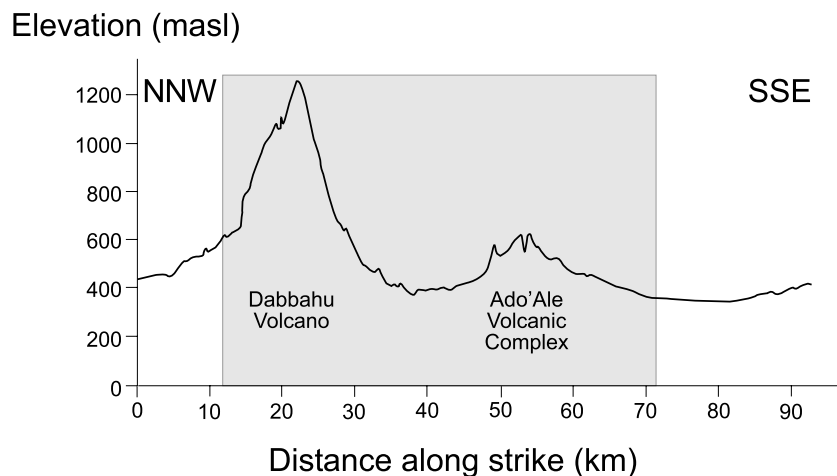
Figure 3. Along-axis topographic profile (A) showing the main volcanic loads in the rift and the region (grey shade) over which seismicity was distributed throughout the period 19 October–17 November. Location of profile is shown in Fig. 2.

Differences between the observed intrarift fracture pattern in the northern DMS and analogue models of oblique rifting may be attributable to the presence of magma (e.g. Clifton & Schlische 2003).

Faults have a mean length of 1.9 km, however linkage between north- and northwest-trending fault segments has generated en echelon fault zones up to 20 km in length. As a percentage of the cumulative length of all measured faults, almost 60 per cent are down-thrown towards the segment axis, which is defined for the most part by the axial graben. Nonetheless, fault facing tends to alternate to some degree across the rift segment and, as a consequence, full grabens occur on the segment flanks. Faults, and their associated fissures, are very closely-spaced ($\ll$500 m) within $\sim$7 km of the rift axis, coextensive with the youngest basaltic lava flows. In this region, remote quantification of cumulative brittle strain is precluded because the geomorphic signature is below the resolution of the currently available 3 arcsecond 90 m resolution digital elevation model (DEM) generated by the NASA Shuttle Radar Topography Mission (SRTM) (Farr & Kobrick, 2000). A photographic transect across the central DMS, to the immediate north of Ado'Ale, is shown in Fig. 6 to illustrate qualitatively the structural morphology of the axial zone.

At the surface the faults are vertical, or near-vertical, have throw and opening displacements (commonly <20 m and 1–3 m, respectively) and show no evidence of frictional contact between the fault surfaces (Fig. 7A). In each case, the surface outcrops of the vertical faults have formed initially by the opening of pre-existing cooling joints. Deep fissures are common between footwall and hanging wall blocks. In some cases, fissures have operated as conduits for the transport of mafic magma: small basaltic constructions are localized on fissures, and flows (some clearly very young), are observed to originate from fissures (Fig. 7B). Fault segments are either linked along strike via breached ramps or reduce throw towards their lateral tips where they terminate in fissures.

Deformation is completely different on hanging wall and footwall fault blocks. Footwall cut-offs are mostly subhorizontal, with only subtle undulations along strike. In contrast, hanging walls record localized 3-D strain effects; strata immediately adjacent to the fault commonly is bent into a series of monoclines with an along-strike wavelength $\ll$ fault length (Fig. 7C). Pressure ridges, or buckles, are common at the base of monoclines. Similar fault morphology has been documented in other areas around the world, including the Main Ethiopian Rift (Acocella *et al.* 2003), the rift zone in Iceland (Gudmundsson 1992; Angelier & Bergerat 1997; Grant & Kattenhorn 2004; Tentler 2005), the Koae fault system in Hawaii (Peacock & Parfit 2002; Holland *et al.* 2006; Martel & Langley 2006), and the Hat Creek fault in northern California (Muffler *et al.* 1994). Although it is agreed that such fault morphology arises as a consequence of slip along less steeply dipping normal fault planes at depth, there are conflicting hypotheses as to whether these normal faults propagate up to the surface from below or vice versa (see Grant & Kattenhorn 2004). This paper provides evidence that supports the view that the vertical faults observed at the surface in Afar initiate at depth and propagate towards the surface.

4 2005 DABBAHU RIFTING EPISODE

An account of the early stages of the Dabbahu rifting event is provided by Yirgu *et al.* (2006), and is summarized as follows. On 2005 September 14, an $m_b \sim 4.7$ earthquake signalled the beginning of a volcano-seismic crisis in the DMS. Between September 24 and 26, station FURI (Addis Ababa), recorded nearly continuous seismic activity, including tremor, with the greatest density of seismicity focused around the Dabbahu and Gab'ho volcanoes in the north of the segment. This was followed on September 26 by a small eruption associated with the opening of a 500 m long, 60 m deep, N–S oriented vent on the eastern flank of Dabbahu volcano. Initial analyses of pumice erupted from the vent are consistent with basaltic triggering of a felsic source at depths <6 km (Wright *et al.* 2006).

Between 2005 September 14 and 2005 October 4, 163 earthquakes ($m_b < 3.9$) were reported by the National Earthquake Information Centre (NEIC) to be located in the vicinity of the Dabbahu rift (Fig. 8A). These earthquakes released an estimated combined seismic moment of 6.7×10^{18} Nm (Wright *et al.* 2006), equivalent to an average moment release of 4.3×10^{16} Nm per event. The maximum moment released in any single event was $\sim$0.8 $\times 10^{18}$ Nm. Our estimates of seismic moment are derived using an empirical relation between body wave magnitude, m_b, and seismic moment, M_0, for the central Afar region (Hofstetter and Beyth 2003). Uncertainties are on the order of $\pm$15 per cent. Both the total number of earthquakes, and combined seismic moment release per day reached a peak on September 24 and 25, and decayed exponentially over the remainder of the period (Figs 8C and D). Earthquake focal mechanisms
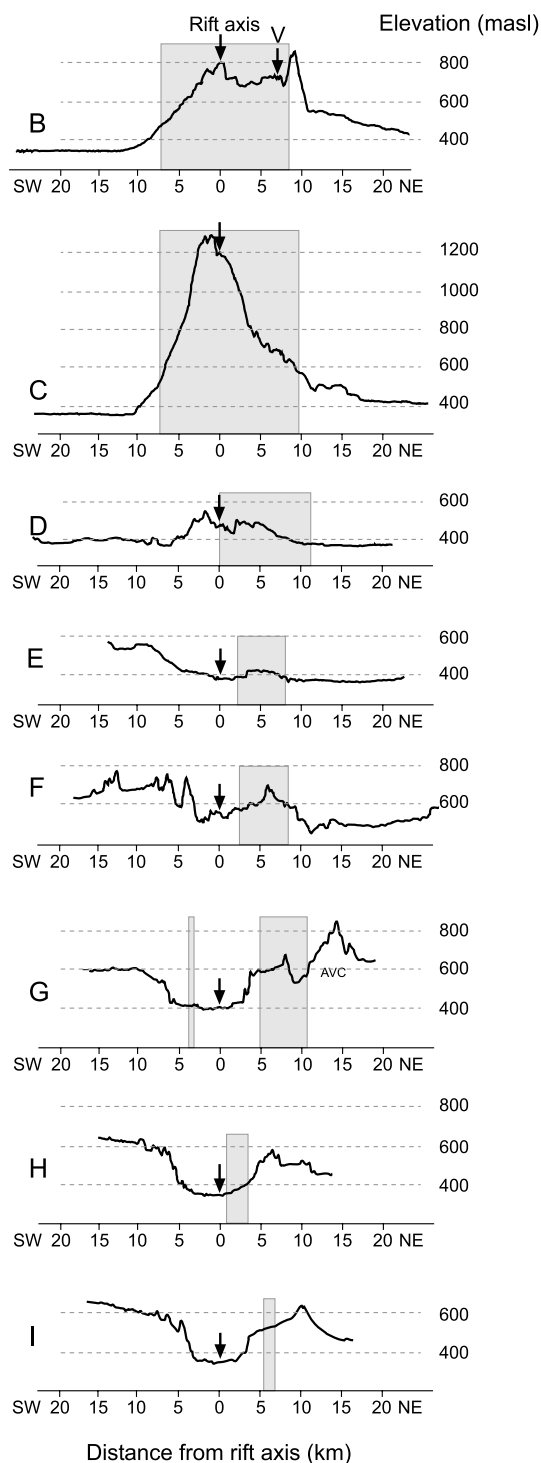
Figure 4. Across-axis profiles showing relief relative to the rift axis, and the width (grey shade) over which seismicity was distributed throughout the period 19 October–17 November. Locations of profiles are shown in Fig. 2. The position of the 2005 September 26 volcanic vent is indicated (V) in Section B.

determined by Harvard CMT predominantly show normal dip-slip perpendicular to the strike of rift faults, with a minority showing varying degrees of right-lateral strike-slip motion (Fig. 8B).

Surface deformation was estimated from 3-D models of satellite radar data (InSAR) spanning the eruptive event (Wright *et al.* 2006; Ayele *et al.* 2007). Uplift reached a maximum of 1.5 m on both rift

flanks, and extended over most of the length of the magmatic segment to a distance of ~12 km either side of the rift axis. Subsidence of up to 2 m developed along a 2–3 km wide zone, located along the eastern flank to the axial graben (Fig. 9D). Maximum horizontal opening at the surface was <6 m, perpendicular to the segment axis except in the vicinity of Dabbahu and Gab'ho volcanoes, where the deformation field was radial, consistent with the pattern expected for deflating magma chambers. This overall pattern of deformation and the distribution of seismicity are consistent with the injection of a large dyke, up to 8 m wide, between depths of 2 and 9 km along the 60 km length of the segment, above which modelled normal faults slipped by an average of ~2 m (Wright *et al.* 2006). In reality, this dyke may comprise multiple injections along the same crustal rupture zone, and its width may be significantly greater at depth. Total geodetic moment release exceeded seismic moment release by an order of magnitude (Wright *et al.* 2006), presumably because magmatic rifting accommodated most of the strain (e.g. Buck *et al.* 2005).

Surface deformation continued during the immediate post-intrusive phase (Figs 9A and B) in response to brittle relaxation in the crust above the zone of dyke intrusion and/or continued injections of magma (Qin *et al.* 2006). In an interferogram spanning this period, fringe discontinuities are apparent to the east of the axial graben and represent either topographic artefacts or recent fault ruptures (e.g. Feigl *et al.* 2000). Ambiguity arises because interferograms are calculated at a resolution in excess of that of the available DEM. Fault scarps that are below the resolution of the DEM are not corrected for during processing, leading to topographic artefacts in the final image. An interferogram of the region before the initiation of rifting was inspected to test for such artefacts (Fig. 9C). Several small artefacts are apparent, the largest of which is defined by a fringe discontinuity of less than one third of a colour cycle (<1 cm movement in the viewing direction of the satellite). However, since aerial inspection demonstrates that small faults are ubiquitous across the entire Dabbahu axial zone (Fig. 6), a broader distribution of fringe discontinuities than is observed should occur if topographic artefacts were a significant problem. The region encompassing fringe discontinuities in the mid-October to mid-November interferogram is, therefore, treated as a zone of active faulting and is delimited using fringe discontinuities of greater than one third of a colour cycle (Fig. 9B).

Although epicentral locations for the September teleseismic events described in Yirgu *et al.* (2006) and Wright *et al.* (2006) are too imprecise to compare with recently active faults, local seismicity patterns from a network deployed 1 month after the onset of activity provide excellent constraints (Ebinger *et al.* 2006). Temporal patterns of seismicity from October 19 to November 17 show repeated swarms concentrated along the eastern side of the rift, including seismic tremor (Ebinger *et al.* 2006), coextensive with the zone of faulting inferred from interferograms spanning this phase of the episode (Figs 9A and B) and the zone of subsidence associated with the initial intrusive phase (Fig. 9D). However, there is a significant reduction in the frequency of seismic events in the following months of 2005 December and 2006 January.

Since the initiation of rifting in 2005 September, further intrusive events have occurred within the DMS. Keir *et al.* (2006b) describe vigorous seismic activity commencing 2006 June 17, which was coextensive with a ~15-km-long region of deformation (2 m of opening) in the centre of the segment, as deduced from satellite radar data. This repetition of intrusive events may signal the beginning of a protracted sequence, similar to that observed from 1975 to 1984 at Krafla, Iceland (Buck *et al.* 2006).
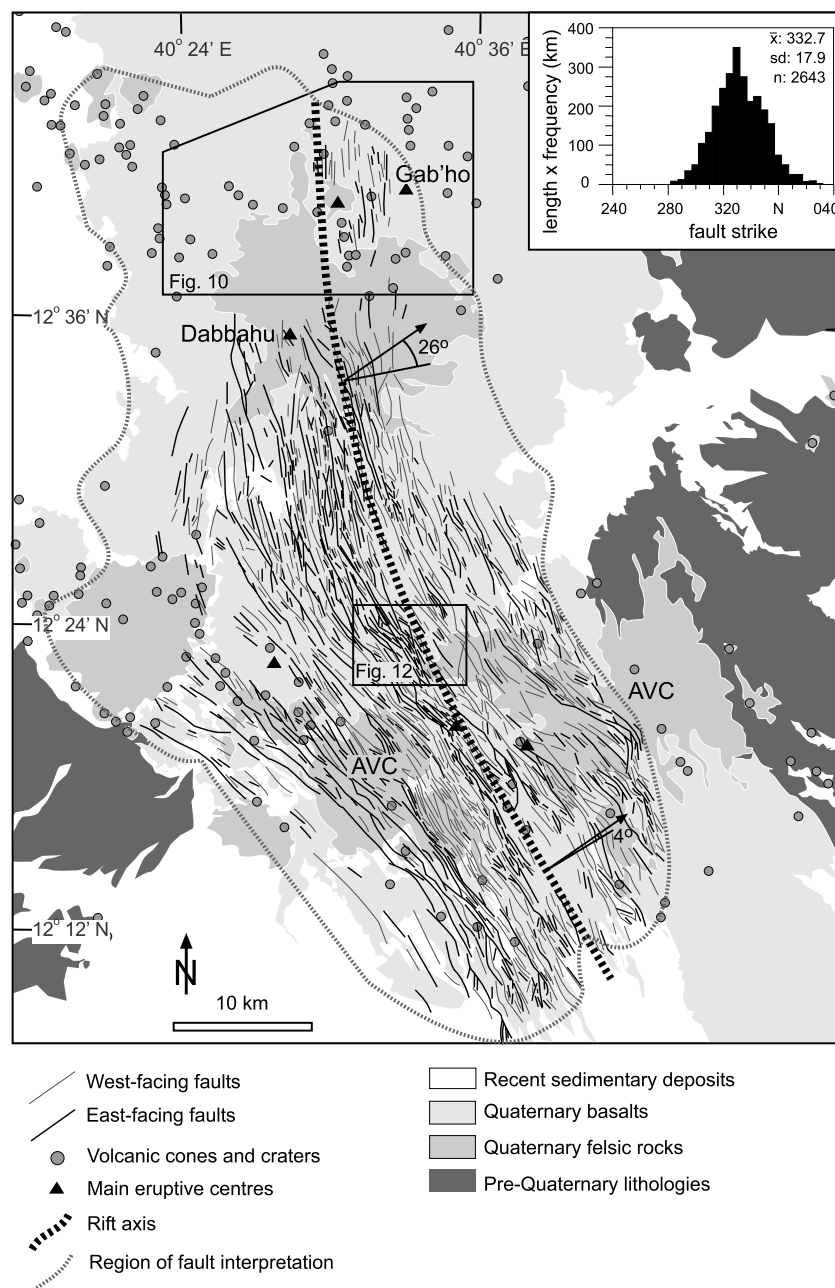
Figure 5. Simplified structural map of the Dabbahu magmatic segment from analysis of large format camera and Landsat imagery (after Hayward 1997). Rift obliquity is shown by the angle between the extension direction (after Jestin *et al.* 1994) and the normal to the rift axis. To the north of AVC, rifting is oblique whereas to the south of AVC rifting is near-orthogonal. Histogram shows fault strike, weighted by length, versus frequency for all faults documented within this region. AVC = Ado'Ale Volcanic Complex. Insets show locations of Figs 10 and 12.

5 FIELD OBSERVATIONS OF BRITTLE STRAIN

Fieldwork was conducted 1 and 6 months after the 2005 September initiation of the rifting episode. Only the northern part of the DMS, near the vent site, was visited in October because the spatial scale of the event was as yet unknown in this sparsely populated region. The second visit targeted areas of most intense seismicity within the initial subsidence zone defined by radar interferometry (Fig. 9D) (Wright *et al.* 2006).

Given the highly fractured and fissured morphology of the DMS, it was important to develop criteria to estimate when the observed surface disruption occurred. A number of observations allow qualitative assessment of the relative age of surface features, including the presence of light coloured sediments on the surface of cooling joints, unweathered surfaces of broken rock, and dead or dying acacia trees and other plants in fissures at the foot of scarps. The first criterion is not intuitive; most fresh surfaces exposed along fault scarps are clean (e.g. Clifton *et al.* 2002). However, the Afar depression is dusty and subject to katabatic winds descending from the adjacent 3-km-high highlands. Aeolian sediments settle in ground cracks, which are mostly subvertical cooling joints in basalt, and to a lesser extent, felsic volcanic lavas. Thus, freshly exposed surfaces of cooling columns are covered in a thin veneer of sediment. In
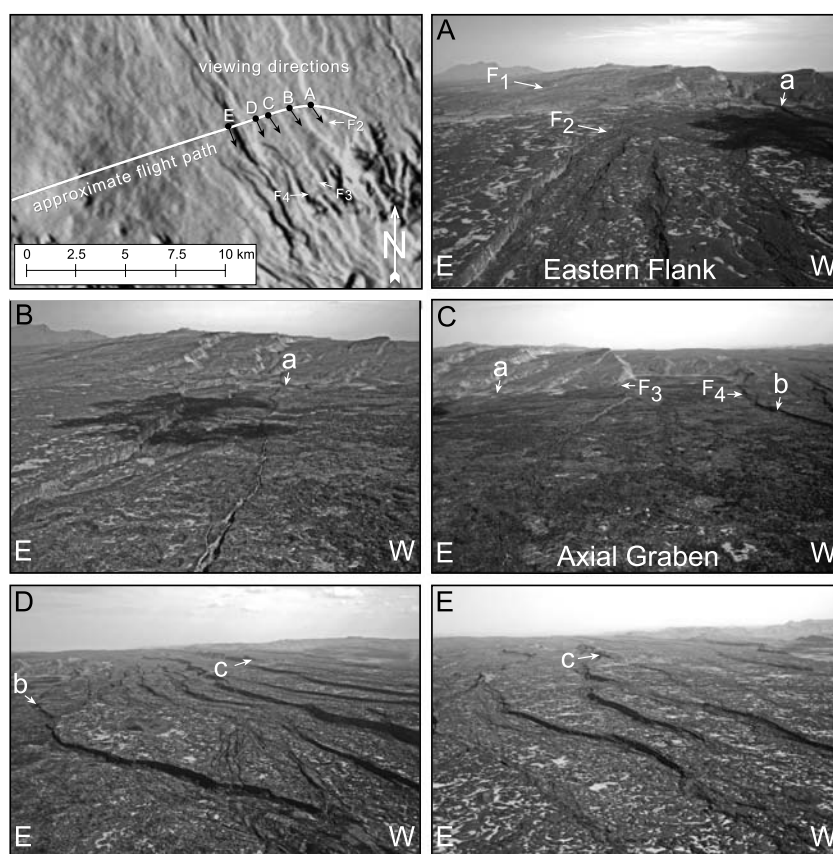
Figure 6. Oblique aerial photographs from east (A) to west (E) across the densely faulted central Dabbahu magmatic segment (structural interpretation shown in Fig. 12). Inset at top left shows flight line (also shown on Fig. 2) and viewing directions for each image. Faults that were inspected in the field and that are discussed further are labelled F_1 to F_4 on inset and photographs. Tie points between images are labelled (a)–(c). Foreground in each image is composed of basalt flows. Dissected dome in background of (A)–(C) forms the eastern sector of the Ado'Ale Volcanic Complex. Dark area on images (A) and (B) is cloud shadow.

contrast, surfaces subjected to the abrasive effect of katabatic winds are free of sediment. This is an extremely useful, if time-limited, tool because of the tendency of faults and fissures to open along pre-existing cooling joints.

Remote inspection of structures across and along the length of the central DMS was provided by helicopter support courtesy of the Ethiopian Air Force and the Ethiopian Ministry of Capacity Building. This, together with on-the-ground inspection, allowed identification of the extent of ground damage. Light-coloured horizons representing fresh rupture surfaces were visible from the air along the base of fault scarps on the eastern flank (Fig. 6B). Similar features were not observed on the western flank or within the axial graben, where fissures and faults were seen to host green trees and shrubs. Three sites within the rift segment were inspected to confirm aerial observations and to test the validity of the surface deformation models (Wright *et al.* 2006) and epicentral locations. Two sites were selected from within the deformation zone defined by radar interferometry (vent, eastern flank) and the third site targeted the axial graben immediately north of the Ado'Ale volcanic complex (Fig. 9D).

5.1 Vent area

The vent punctured through a volcaniclastic basin at the southern margin of an obsidian dome (Locality 1, Figs 10 and 11A) and ejected clasts up to 0.5 m in diameter. These were distributed up to 200 m from source. A small volume of peralkaline rhyolite was extruded subsequently in a rent at the northern end of the vent. Fissures occur on either side of the vent in both the volcaniclastic basin and in an obsidian flow. In the basin, fissures occur in swarms with individual cracks having small heaves (horizontal opening) of <50 cm that together yield a cumulative opening of >3 m over a horizontal distance of ∼15 m. Vertical offsets are variable (<80 cm) with greatest throw on individual cracks occurring where the fissure swarm simplifies to fewer structures. In contrast, single, wide (up to 5 m) fissures predominate within the obsidian flow. Vertical offset was difficult to assess because of the topographic variation on the original obsidian flow surface but was less than a few metres.

About 500 m east of the vent, a west-facing fault trends towards 346° and forms the eastern boundary to the volcaniclastic basin described above. This fault is soft-linked to the north with a fault of larger displacement (up to ∼50 m), which cuts through an obsidian dome (Figs 10 and 11A). Local pastoralists reported ∼1 m of offset along a segment of this fault on the day of the vent eruption (Yirgu *et al.* 2006). In total, up to 5 m of fresh vertical displacement accrued on the southern fault segment at Locality 2 (Figs 10 and 11B). Here, the obsidian footwall is loose and blocky and fresh rock fall is abundant. A series of open fissures, pits and grabens developed within the volcaniclastic sediments of the hanging wall to a distance of 21 m away from the fault (Fig. 11C). There is a small right-lateral component of shear across fissures at their lateral tips. Note though, that within an along-strike distance of a few meters,
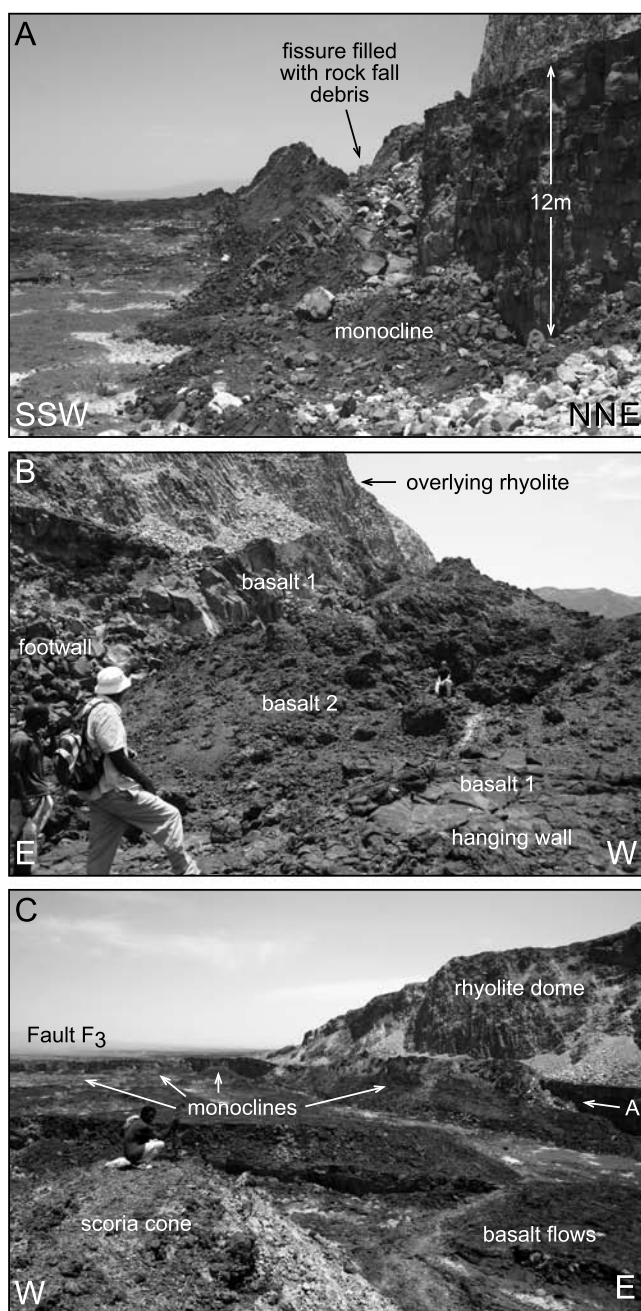
Figure 7. (A) View to NNW along a vertical fault (F_3) in the axial graben showing the morphology typical of normal faults in the Dabbahu segment. (B) View south towards fault F_3 showing a localized outcrop of young scoriaceous basalt contained within the fissure. (C) View north towards Fault F_3 showing the development of monoclines in the hanging wall to the fault. Notice the subhorizontal footwall cut-off compared with the undulating hanging wall cut-off. Viewing direction for (A) is arrowed.

the opening vector is orthogonal to the overall fissure trend; the strike-slip component appears to be related to the change in crack mode at the propagating tip (Pollard *et al.* 1982), and therefore, is not indicative of the regional kinematics. Total vertical offset of ~5 m also occurs in the region of fault-linkage with the northern segment, though a component of this offset is accommodated by monocline development in the hanging wall (Locality 3, Figs 10 and 11A). Continuation of fault slip to the north is likely given the distribution of seismicity and the presence of open fissures in the hanging wall,

which were observed from a position at the top of the footwall adjacent to Locality 4 (Fig. 10 and 11A). According to local observers, 2 days before the volcanic eruption sulphurous gases vented from this fault in the vicinity of Locality 3 (Yirgu *et al.* 2006). In 2006 March venting was not observed here or further south, though the fault at Locality 4 clearly localizes hydrothermal fluid; an acid-sulphate hydrothermal system occurs in its footwall and fumeroles (boina) are exploited by the local Afar pastoralists for steam condensate.

5.2 Eastern flank

Numerous west-facing faults and smaller conjugate structures were active on the eastern flank during the Dabbahu episode (Fig. 12). Older scarps with fresh offset at their base are clearly visible in the oblique aerial photographs because of the contrast in colour between clean and freshly exposed, sediment-coated rock (e.g. Fault F_2, Fig. 6A). These faults are continuous along-strike for at least several kilometres, and were observed to dissect the Ado'Ale volcanic complex in the central region of the DMS. An east- and west-facing pair of such structures is described below, together with a region of intense dilation.

Fresh fault slip is visible at the base of a NW-trending, east-facing scarp that cuts across a rhyolite dome (Locality 5, Figs 12, 13A and B). The northwestern lateral tip of the structure runs into a basaltic flow field, covered to depths of ~30 cm with a layer of volcaniclastic sediments, where it is expressed as a series of deep fissures (Figs 13A and C). During the Dabbahu episode, vertical displacement of 2.7 m (local value) accrued where the fault cuts the dome. In combination with the pre-existing scarp height, this yields a total offset of ~20 m. In contrast, there was no pre-existing scarp within the basalt flow field, which has relatively flat topography. Vertical offset is much reduced across individual fissures (50 cm horizontal and 30 cm vertical offset on average), though some cracks accommodate significantly more displacement locally over short, along-strike distances (Fig. 13C). Opening directions ($050° \pm 5°$) were determined in several places by matching columns across the fissures. This direction is slightly east of the predicted kinematic extension vector ($044°$) determined using recently acquired GPS data (Vigny *et al.* 2006) and may be attributable to a change in crack mode towards the propagating lateral tip of the fault, as discussed earlier. Since the structures are subvertical, small irregularities in the dip of the fault produce significant changes in the kinematics of the structure. For example, oversteepening of the fault, such that it dips towards the uplifted block, induces localized zones of convergence, which are accommodated by the development of small-scale reverse faults in the hanging wall (Fig. 13D).

The west-facing fault at Locality 6 (Fig. 12) offsets basalt and developed along a pre-existing structure, which had an associated rubble-filled fissure prior to the Dabbahu episode (Fig. 14). Aerial inspection reveals that this fault ruptured over a strike length >2 km; fresh slip is visible on the lateral continuation of the structure through the Ado'Ale volcanic complex to the south (Fault F_1, Fig. 6A). A 200 m transect along the fault in the vicinity of Locality 6 revealed that although the recent event mostly reactivated the earlier fault, in places a new rupture broke through either the hanging wall or footwall to the pre-existing scarp. Fresh vertical offset is on the order of 2–3 m, as measured using the displacement of the thin layer of pyroclastic sediments that mantle the basalts, and the width of freshly exposed basalt columns (Fig. 14A). Fresh horizontal opening is difficult to constrain but, given the width of the fissures at the base of the scarp, is likely to be <2 m. Monoclines are well-developed
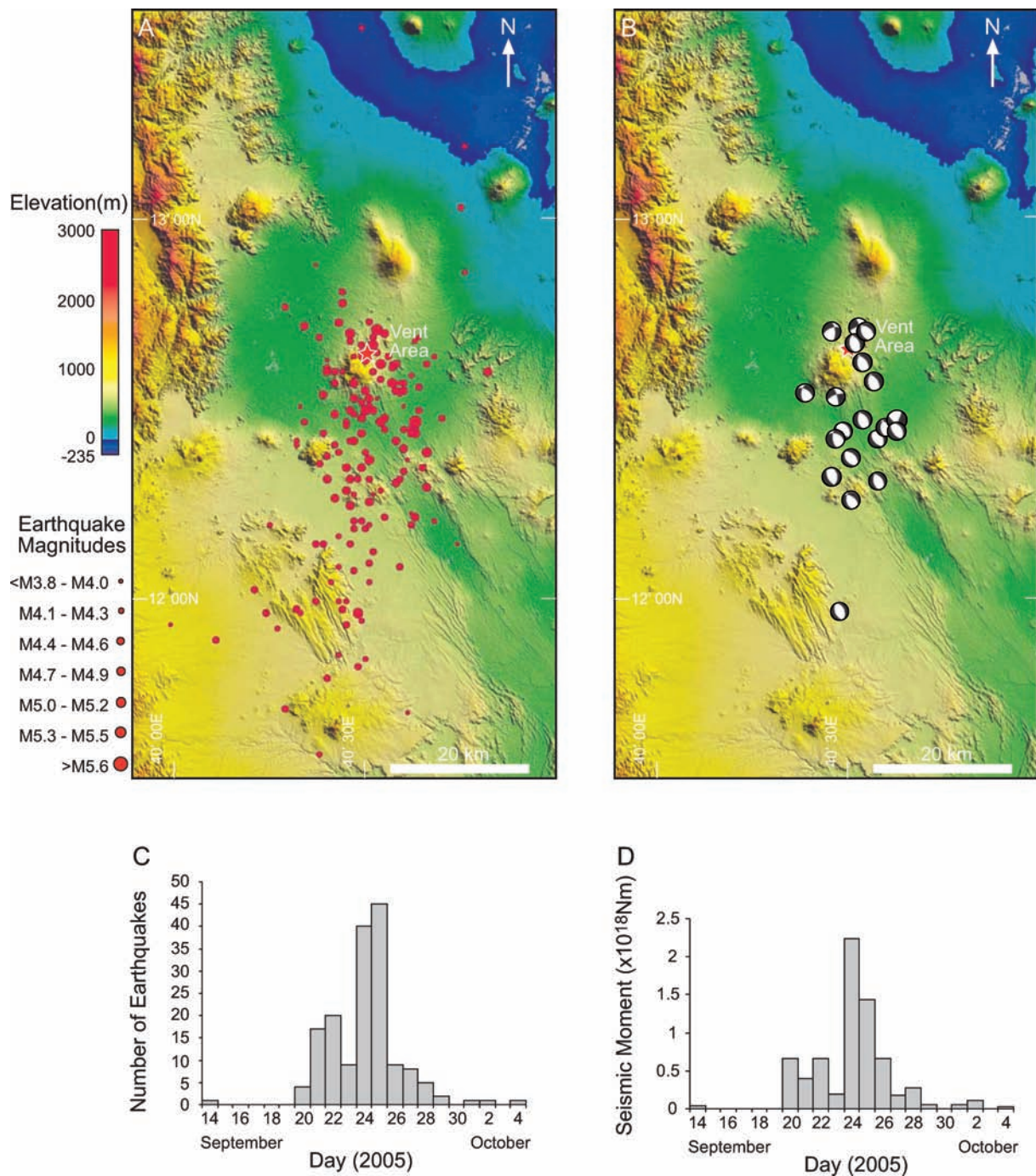
Figure 8. 90 m SRTM Digital elevation model of the Dabbahu Magmatic Segment and surrounds showing (A) the distribution of earthquakes reported by NEIC between 2005 September 14 and October 4 (red circles scaled according to magnitude), and (B) earthquake focal mechanisms determined by Harvard CMT. The histograms show (C) earthquake frequency per day and (D) combined seismic moment released per day.

along the hanging-wall, with the basalt flow surface dipping up to 40° away from the fault (Fig. 14B). Vertical displacement between footwall and hanging wall cut-offs is much reduced (approaches zero) where monoclines are present. Total throw, measured as the combination of displacement between footwall and hanging wall cut-offs and the height of the monocline, remains much the same along most of the fault in this vicinity. Compressional effects occur within the hanging wall and are expressed as push-ups along minor thrust faults, and pressure-ridges. All observed compressional structures occur at the base of monoclines (Fig. 14C).

Fault F_2 has a local throw ∼6 m and occurs at Locality 7 (Fig. 12). This west-facing fault forms a ∼2-km-long segment in a linked en echelon fault zone that comprises several similar scale segments and extends north towards Dabbahu volcano. An east-facing fault is located 200 m to the west of Fault F_2, and together the pair form a small graben. Dilation within this graben and in its surrounds is exceptional; columnar joints in the basalt host-rock have opened across the entire zone. The instability of the hanging walls and the scale of the associated fissures precluded close inspection of the fault scarps. However, the morphology of footwall and hanging wall
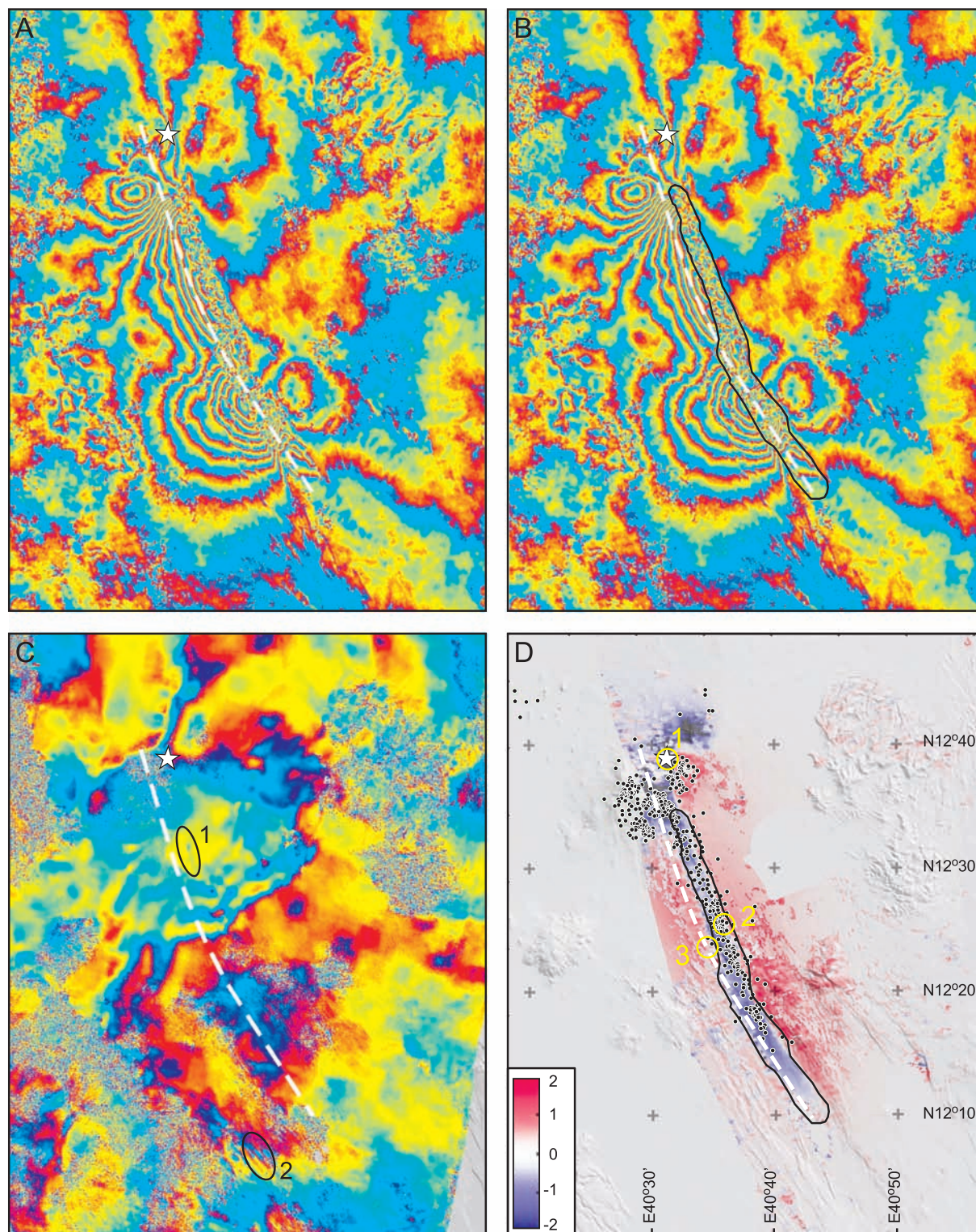
Figure 9. Surface deformation associated with the Dabbahu episode from mid-September 2005 to 17 November 2005 covering the major intrusive and associated post-intrusive phase in the 2005-to-present rifting episode. All images are of the same region at the same scale. Rift axis shown by dashed line, vent shown by star. (A) Wide-swath interferogram spanning the period 13 October–17 November 2005. Each colour cycle (magenta-cyan-yellow-magenta) represents a range increase of 2.8 cm. Range increases signify relative subsidence and/or eastward motion in this ascending interferogram. (B) Region of fault activity in (a) is delimited by fringe discontinuities >1/3 colour cycle. (C) Pre-rifting interferogram of the same region constructed to check for topographic artefacts. Very few linear fringe discontinuities occur and those that do (circled, 1 and 2) have a maximum magnitude of one-third colour cycle. (D) Initial subsidence during the major intrusive phase (blue area) inferred from satellite radar data (Wright *et al.* 2006), overlain by the region of faulting inferred from (B) and the distribution of seismicity (Ebinger *et al.* 2006) associated with the post-intrusive phase (black dots). Field inspection areas: 1, vent region; 2, eastern margin; 3, axial zone.
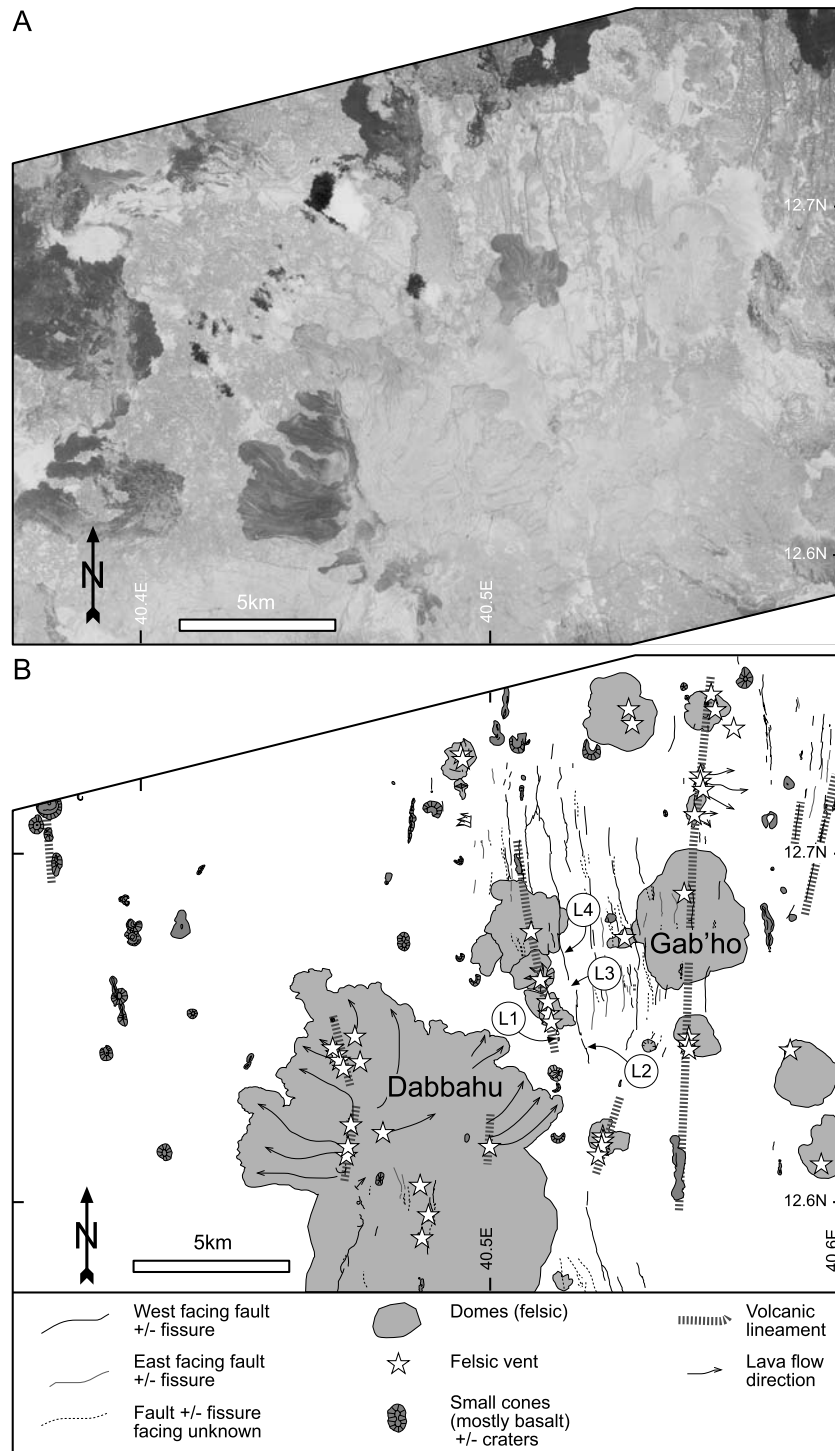
Figure 10. Vent area. (A) Corona Image, acquired c. 1965, showing the northern flanks of Dabbahu Volcano and the vent area. Image supplied courtesy of the Fault Dynamics Research Group, Royal Holloway. (B) Interpretation of CORONA image at a horizontal resolution of ~2.5 m pixel^{-1} showing the main tectono-magmatic features in the vent area. Localities discussed in text are labelled. Note the preferred alignment of volcanic features parallel to the tectonic grain.

blocks can be matched across the fissure to yield opening vectors. Total displacement is predominantly dip-slip with a slight right-lateral component on the east-facing fault (Fig. 15). The amount of dilation in the vicinity and the perilous state of the scarps (vis á vis hanging columns on the verge of failure) suggest that these structures

were recently active. Although an assessment of the amount of fresh slip on these faults is equivocal at this locality, inspection of oblique aerial photographs reveals the presence of a 1–2-m-wide horizon of light-coloured sediment indicative of recent fault activity at the base of the F_2 scarp a few hundred meters to the north (Fig. 6A).
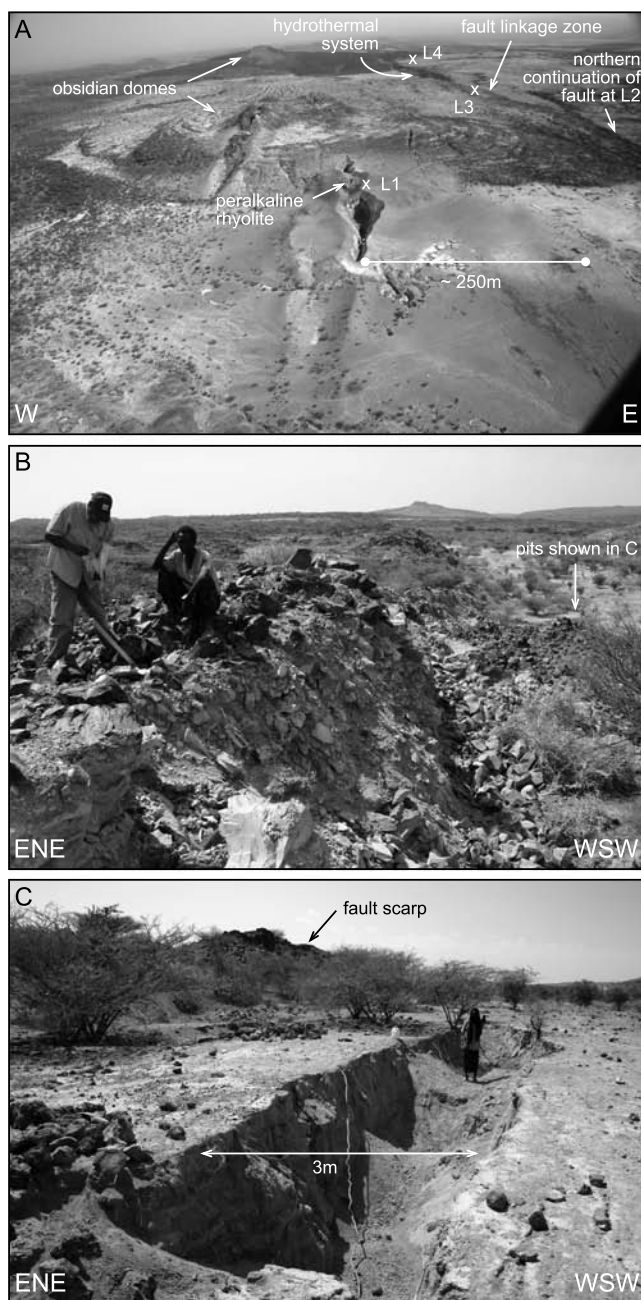
Figure 11. (A) Oblique aerial photograph of the vent area, viewed to the north. The light grey material that covers the ground around the vent comprises ash and clasts ejected during the eruption. Localities discussed in the text are annotated. (B) View to the south along the strike of a normal fault proximal to the vent at Locality 2 (Fig. 10), showing 5 m of fresh vertical offset across an obsidian flow. (C) Pits developed in volcaniclastic sediments on the hanging wall to fault at Locality 2. Location shown in (B).

5.3 Axial graben

The axial graben was accessed immediately north of the Ado'Ale volcanic complex. This area was aseismic in the period 2005 October 19–November 17 (Fig. 9), and radar interferometry shows no localized fault offsets (Wright *et al.* 2006). The area largely is covered by a'a basalt lava flows, interspersed with flatter regions of pahoehoe lava. Two graben-bounding faults were inspected, both of which dissect the dome, as was the intervening axial zone.

Fault F$_3$ (Figs 6C and 7; Locality 8, Fig. 12) bounds the graben to the east, offsets the surface of the basalt flow field by about 20 m and was impassable because of the lack of accessible ramps and the presence of a well-developed fissure at its base. Although rock fall is prevalent along the scarp, particularly at the intersection with north-trending fractures, diagnostic evidence for fresh offset was not observed. Trees are growing in the associated fissure and show no signs of distress, as would be expected, and indeed was noted elsewhere, had the fault ruptured during the Dabbahu episode. This structure has acted as a conduit for mafic magma in the past, as indicated by the presence of small basalt hornitos within the fissure (Fig. 7B).

Fault F$_4$ (Fig. 6C; Locality 9, Fig. 12) bounds the axial graben to the west, offsets the surface of the basalt flow field by 8–10 m and has a significant amount of recent rock fall along its base, filling small fissures and extending out onto the hanging wall block. As observed along Fault F$_3$, and noted elsewhere during aerial inspection, rock fall is enhanced at fault intersections and linkage zones. Fissures are not well developed in this vicinity, and where present are largely filled with rubble spalled from the scarp prior to the Dabbahu episode. Columnar joints in the hanging wall are, for the most part, tight; there is very little evidence for dilation along this structure. Notwithstanding a possible zone of slip (throw ~30 cm) at the intersection with a rhyolite dome of the Ado'Ale volcanic complex, Fault F$_4$ does not appear to have ruptured during the Dabbahu episode.

The blocky and fractured character of the a'a lava in the axial zone tends to obscure fissures unless they are of a scale that is greater than the dimensions of the individual slabs of basalt. Fissures of such a length were not observed in the a'a lava field. On the other hand, fissures do occur within the pahoehoe lava, but they generally form variably oriented rents across the top of small (<10 m diameter) lava domes. These are interpreted as having developed as a result of the cooling of magma 'blisters' during emplacement. The few fissures related to the Dabbahu episode that were noted along the transect across the axial zone occurred within sediment-filled depressions in the basalt field and had horizontal openings <5 cm.

6 DISCUSSION

6.1 Distribution of brittle strain

Our observations verify the pattern of brittle deformation predicted in 3-D models of satellite radar data (Wright *et al.* 2006; Ayele *et al.* 2007). Field and aerial investigations reveal a ~5 km-wide zone of open fissures, monoclines, and subvertical normal faults with up to 3 m of recent displacement, along much of the eastern flank to the north of Ado'Ale volcanic complex. Vertical displacements of up to 5 m occur on faults proximal to the vent that erupted on 2005 September 26. Although horizontal openings were difficult to assess on pre-existing fissures, we found <3 m cumulative opening on a new fissure swarm near the vent, and ~30 cm opening on new fissures on the eastern margin. These preliminary measurements are relevant because they capture a component of strain that may well be irresolvable if the structures are subsequently covered by late-stage extrusive lavas.

Since field observations of recent ground breaks show good spatial correlation with the distribution of seismicity recorded during the period October 19–November 17 (Ebinger *et al.* 2006), this seismic data set is treated as a proxy for the surface distribution of brittle strain throughout the region. Over much of the length of the
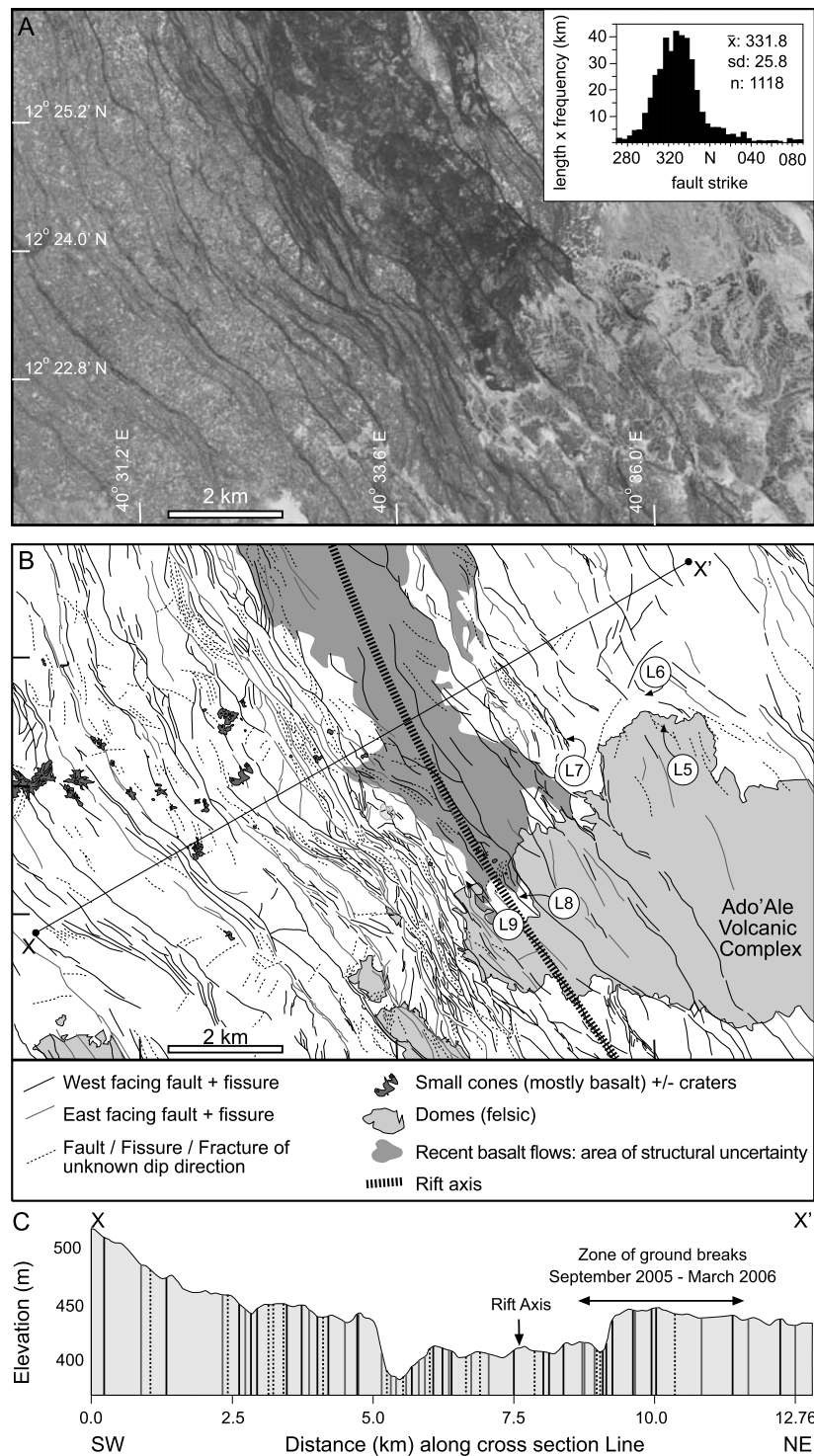
Figure 12. Central Dabbahu magmatic segment. (A) Corona Image, acquired c. 1965, showing the central Dabbahu magmatic segment in the vicinity of the dissected Ado'Ale Volcanic Complex. Image supplied courtesy of the Fault Dynamics Research Group, Royal Holloway. Inset shows fault statistics for the interpreted image in (B). (B) Interpretation of stereo-CORONA images at a horizontal resolution of ∼5 m pixel^{-1} showing the main tectono-magmatic features in the vent area. Localities discussed in text are labelled. (C) Structural cross-section from X to X' in (B) showing the density of ground breaks in the central Dabbahu magmatic segment. Topography determined using the SRTM 90-m resolution DEM. Colour-coding of faults is the same as for the map.

segment, the zone of surface brittle strain and maximum subsidence during the 2005 rifting episode extends across a width of <5 km, and is centred up to 5 km east of the axial graben (Fig. 4) (Wright *et al.* 2006). Mechanical models of dyke intrusion demonstrate that the width of induced brittle strain is roughly twice the depth to

the dyke (e.g. Rubin 1992). Taking this ratio as a rule of thumb, our data is consistent with the intrusion of a dyke to depths of <2.5 km, as inferred from the distribution of seismic tremor (Ebinger *et al.* 2006), and the deformation field determined using satellite radar data (Wright *et al.* 2006; Ayele *et al.* 2007). The
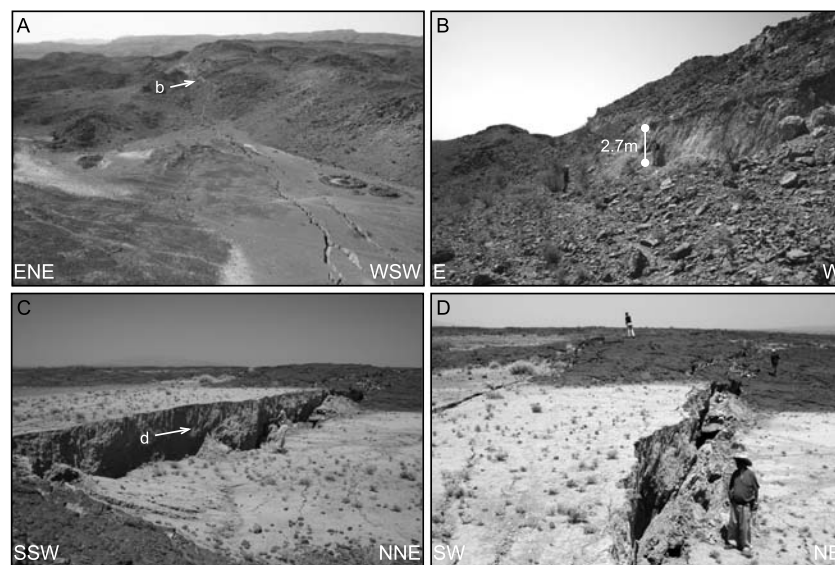
Figure 13. Recent ground breaks on the eastern flank: (A) View to SE, showing the change in failure mode from shearing in the rhyolite dome at Locality 5, to opening mode fissures where the structure's NW-lateral tip cuts a basalt flow field. (B) Detail of the dome in (A) showing 2.7 m vertical displacement. (C) and (D) Detail of fissures in (A) showing a vertical offset <2 m and local compressional effects induced by irregularities in the dip of the subvertical footwall.

localization of strain approximately 5 km to the east of the geomorphic axial graben indicates that melt supply to the crust is not always at the centre of the rift segment. Nonetheless, on geometrical grounds the axial graben must represent the mean position about which dykes are intruded, in which case the width of the melt feed zone exceeds 10 km, broader than that expected for slow-spreading mid-ocean ridges (e.g. Buck *et al.* 2005).

The magnitude of fault slip during the Dabbahu episode demonstrates the importance of dyke intrusion to the development of rift-zone geomorphology and topography (e.g. Rubin & Pollard 1988). If the distribution of brittle strain associated with this rifting episode is assumed to be typical for the segment over time and is the principal means by which these faults grow, then the minimum number of discrete rifting episodes required to account for the rift geomorphology can be estimated. For example, taking 2–3 m of vertical offset as a typical fault displacement per rifting episode, a scarp height of 18 m, as seen at Locality 5, may represent up to nine magmatic rifting cycles. Topographic data across the DMS is currently of insufficient resolution to adequately capture faults for this purpose, nor do we know the rate of topographic resurfacing by lava production. Nonetheless, a first order estimate can be obtained by assuming an average fault spacing (200 m) and throw (10 m) across the 15 km-wide segment. If a width of 5 km is activated in any single rifting episode, then <400 rifting episodes could account for the observed topography across the segment. If it is also assumed that the maximum horizontal opening (6 m) estimated for the 2005 rifting episode is a representative value, then one rifting episode every *ca.* 400 yr is sufficient to accommodate the time-average opening rate of 16 mm yr^{-1} (Chu & Gordon 1998). As a minimum estimate, the topography of the Dabbahu rift segment may have developed in *ca.* 200 ka.

6.2 Fault scaling relationships

Preliminary field observations provoke questions regarding the general applicability of empirical fault scaling relationships to fault growth in magmatic rifts, a notion that will be tested quantitatively in subsequent work. Fault displacements during the Dabbahu episode are higher than expected for typical tectonic earthquakes based on empirical scaling relationships. If it is assumed that the maximum displacement recorded on individual faults is 2–3 m, as our field work suggests, then from inspection of regression curves for a global suite of normal fault data from continental rifts, one would have expected earthquakes of magnitude >$M_{6.5}$ (Wells & Coppersmith 1994). This is an order of magnitude greater than the largest earthquake recorded during the Dabbahu episode. Empirical slip to length relationships fit our observations better providing we define rupture length as the length extent of the zone of brittle strain. Anomalous fault scaling relationships are not isolated to the Dabbahu case. A low seismic moment to slip ratio was also observed during the Krafla magmatic rifting episode, Iceland (Brandsdóttir & Einarsson 1979).

Several factors may contribute to the discrepancy between field observations and expected fault scaling relationships. First, slip may accrue incrementally over the duration of the rifting episode (e.g. Smith *et al.* 1996). Studies of exposed mafic intrusions in other settings demonstrate that dykes are generally on the order of 1–2 m wide (e.g. Forslund & Gudmundsson 1991). Given the dimensions of the modelled intrusion in this episode, a number of discrete injection events likely contributed to the total dyke opening. Thus, successive dyke injections may have reactivated the same structure in the overlying brittle cap; fresh slip at the foot of a fault scarp may represent several co-intrusive displacements. Limits can be placed on the likely number of slip events required to account for the observed maximum displacement using the few cases where slip is known for a single event. For example, a fault to the northeast of the vent was observed to slip >0.5 m (Yirgu *et al.* 2006). If this is a typical displacement per event, one may reasonably expect that <10 such events are required to account for the maximum fault displacement of 2–3 m. Unfortunately, recognition of multiple slip events on individual scarps over such a short time interval is beyond the resolution of our field and remote techniques. Microseismicity
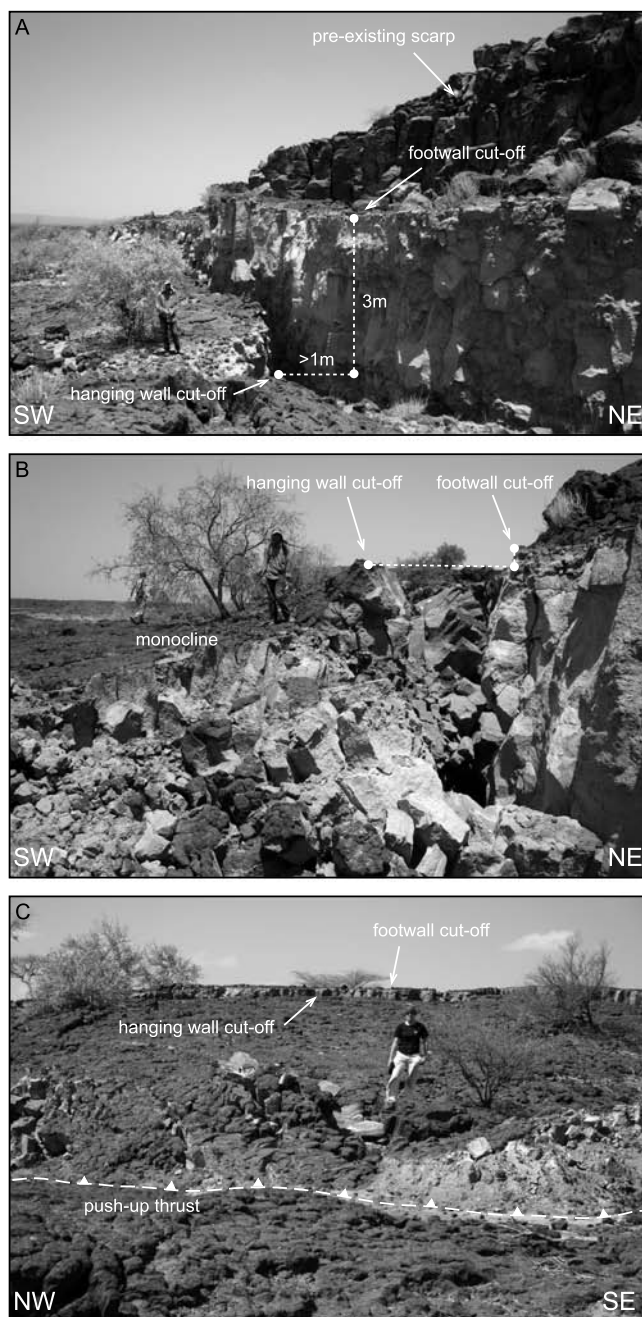
Figure 14. Fault F_1 on the eastern flank at Locality 6. (A) Fresh offset indicated by a colour change on the scarp. Note the dead acacia tree on the hanging wall and the presence of a pre-existing scarp. (B) Monocline development in the hanging wall to the fault. Note the reduction in vertical offset between footwall and hanging wall cut-offs. (C) View orthogonal to the fault scarp showing a well-developed monocline and associated compressional structure at its base (push-up thrust). The fault scarp is visible in the distance.

patterns are being used to investigate the occurrence of repeat episodes of intrusion and fault reactivation.

Secondly, if dyke intrusion involves lateral propagation as expected here from preliminary analyses of the time-distribution of earthquake hyocentres, then faults above and ahead of the intruding dyke may be expected to increase in length during emplacement (Smith *et al.* 1996). Lateral dyke propagation is presumed to occur at rates of a few tens of centimetres per second (e.g. Brandsdóttir

& Einarsson 1979), and with zones of induced tension extending above and several kilometres ahead of the propagating tip (Rubin & Pollard 1988). Emplacement along a 30-km strike length could take a day or more, inducing lateral fault growth by segment linkage over a similar time scale. Fault displacement on longer faults may then include slip associated with the rupture of individual fault segments, which scales with seismic moment, and perhaps a slow slip component that accumulates as the fault lengthens, which is effectively aseismic. A preliminary assessment of the interferogram that spans the immediate post-intrusive phase (Fig. 9a), indicates up to 10 per cent after-slip in the initial subsidence zone. However, this may be attributable to either continued dyke intrusion or relaxation of the brittle crust above the level of intrusion.

Thirdly, scaling relationships between various fault parameters for earthquakes induced by lateral dyke propagation may differ from those established for purely tectonic events. Fault slip can be estimated for typical fault segment lengths using the equation for static seismic moment (Aki 1966),

$$M_o = \mu \Delta u L W, \tag{1}$$

where Δu is the average fault slip, L is fault segment length, W is fault width and μ is the shear modulus of the source region, which is usually taken as 30 GPa for crustal faults (Hanks & Kanamori 1979), but may be an order of magnitude lower in volcanic rifts (e.g. Rubin & Pollard 1987). Assuming 2 m is the average coseismic slip, and taking the average seismic moment released per event as an upper limit to that released by most earthquakes during dyke emplacement, then rupture area is unusually small. At Dabbahu, continuity of fresh slip can be observed on segmented faults over lengths of >10 km along the eastern rift margin, but rupture lengths and widths associated with specific seismic events are unconstrained. Nonetheless, taking the average segment length of 1.9 km as a representative value for L, and letting $\Delta u = 2$ m, which was towards the low end of observed fault displacements, the average seismic moment release per event (4×10^{16} Nm), could be produced if rupture width ~ 300 m. Such L/W ratios are reasonable for small faults induced ahead of and above a dyke that propagates laterally within the upper crust. Longer fault segment lengths result in unusual L/W ratios compared with purely tectonic events (e.g. Mohammadioun & Serva 2001). For the above example, if $L = 10$ km then $W = 70$ m. The effect of a decrease in the shear modulus, say to $\mu = 12$ GPa based on Icelandic estimates (Fiegl *et al.* 2000), would be to increase fault width to 170 m for $L = 10$ km. However, a low shear modulus probably is not warranted in the Afar case, where the Vp/Vs ratio is high (1.8) and $Vp = 4.5$ km s^{-1} for the uppermost 3 km (e.g. Jacques *et al.* 1999).

6.3 A generalized model for development of normal faults within the Dabbahu rift segment

Numerous mechanical arguments and geophysical observations have been put forward to demonstrate that magma intrusion at depth is capable of initiating fault slip and graben formation at the surface (e.g. Brandsdóttir & Einarsson 1979; Rubin & Pollard 1988; Rubin 1992; Chadwick & Embley 1998). Following these arguments, we consider that the fresh ground breaks observed in the DMS developed because of the interaction between far-field tectonic stress and local stresses induced in the surrounding crust by the intruding dyke. The fault growth model we envisage follows that proposed by Tentler (2005) to explain the development of brittle structures within the central rift zone of Iceland (Fig. 16). However, we also incorporate the notion that a rifting episode comprises a sequence

Figure 15. View towards east-facing scarp at Locality 7, showing piercing points for geomorphic markers offset by the structure. Cooling fractures in the basalt host-rock are dilated.

of dyke intrusions, which propagate decreasing distances throughout the episode in response to feedback between tectonic stress and magma pressure (Buck *et al.* 2006).

At a critical moment governed by the balance between the tectonic stress state, defined by three principal compressive stresses $\sigma_1 > \sigma_2 > \sigma_3$, and the internal magma pressure, *Pm*, planar magma-filled fractures initiate perpendicular to the least principal stress, σ_3, and provide conduits for the lateral and perhaps upwards propagation of magma. These Mode I, blade-like fractures originate in conditions of strong magma pressure, such that the effective least principal stress, σ_3, is tensile (negative). If insufficient amounts of magma are supplied to fully accommodate extension, the dyke is emplaced at an effective level of neutral buoyancy within the brittle crust (Lister & Kerr 1991; Buck 2004). This is likely a common phenomenon; intrusive episodes are expected to outnumber extrusive episodes over the duration of the volcanic system. In the absence of overpressured fluids, the stress state in the region above the dyke is compressive. However, the change in horizontal stress within the host rock due to dyke intrusion reduces horizontal compression in a broad region above the dyke, inducing shear failure on normal faults (Pollard *et al.* 1983; Rubin & Pollard 1988; Chadwick & Embley 1998). These faults propagate upwards as discrete planes of failure to shallower crustal levels. As the failure approaches the surface, columnar joints are reactivated as opening mode fissures above the upper tip line of the normal fault zone in response to a high-stress concentration (cf. Grant & Kattenhorn 2004). Eventually, the upward propagating fault zone links with the reactivated fissures to form a vertical fault with opening displacement.

Monoclines are here interpreted as second order structures that develop consequent on fault growth. Various mechanisms explaining their development have been invoked for similar structures in Iceland (Grant & Kattenhorn 2004), the Koae fault system in Hawaii (Holland *et al.* 2006; Martel & Langley 2006), and the MER (Acocella *et al.* 2003). Although some monoclines may develop in association with surface flexure above an upward propagating normal fault (e.g. Grant & Kattenhorn 2004), many of the Dabbahu examples are more planar and slab-like in profile than predicted by this model. We suggest that hanging wall subsidence is a major factor in slab-like monocline development (e.g. Holland *et al.* 2006). Nonetheless, normal fault development at depth consequent on dyke intrusion is the driving process for fissure development at the surface.

6.4 Implications for the evolution of tectono-magmatic segments at slow spreading divergent margins

As recognized previously (e.g. Hayward & Ebinger 1996; Wright *et al.* 2006), and discussed earlier, the DMS is similar in scale and morphology to a slow-spreading ridge. The 2005 Dabbahu rifting episode, therefore, provides insight as to how strain is distributed in space and time at such divergent margins. Many authors invoke alternating phases of magmatism and tectonism consequent on non-steady state accretion to explain the morphology of slow-spreading ridges (e.g. Tucholke & Lin 1994). Since magma bodies are only thought to reside intermittently beneath slow-spreading segment centres, much of the axial valley relief is thought to evolve during periods of tectonic extension (e.g. Curewitz & Karson 1998). However, the spatial and temporal pattern of deformation during the Dabbahu episode demonstrates that a component of axial valley relief can develop in tandem with dyke intrusion. A similar
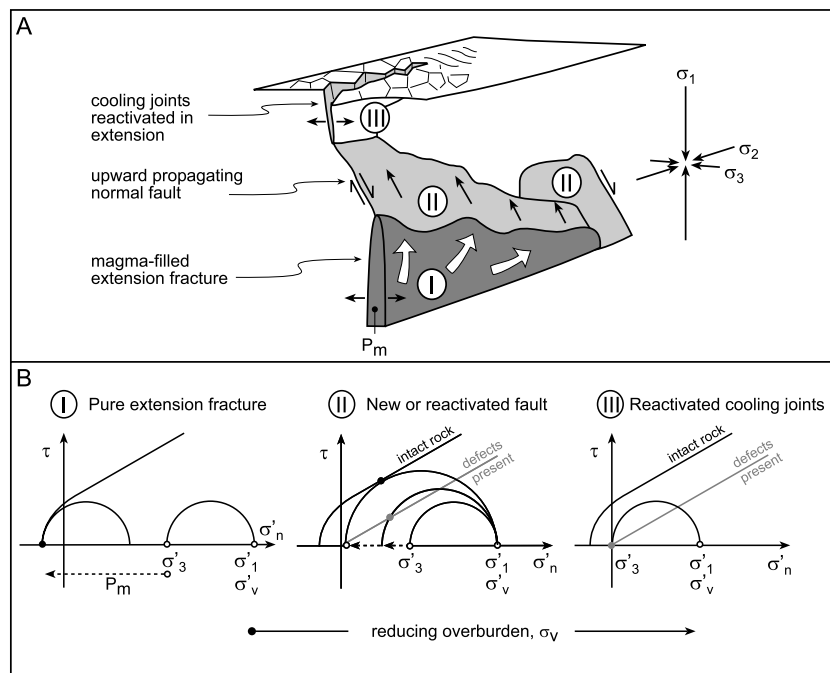
Figure 16. (A) Cartoon showing the development of faults and fissures during a single dyke injection event (after Tentler 2005). I: A dyke injection event occurs at a critical moment governed by the balance between the magma pressure, P_m, and the tectonic stress state, which is defined by three principal compressive stresses $\sigma_1 > \sigma_2 > \sigma_3$. II: Normal faults are initiated or reactivated ahead of and above the laterally and possibly upward propagating dyke. III: Pre-existing subvertical cooling joints are reactivated as opening mode fissures in the region of induced stress above the upper tip line of the normal faults. Once the upward-propagating normal faults and the fissures are fully linked, vertical displacement accrues at the surface. (B) Mohr circles representing the stress state governing the mode of brittle failure at each crustal level are plotted on graphs of shear stress, τ, versus effective normal stress, $\sigma_n' = \sigma_n - P_m$. Failure curves are shown for intact rock and for pre-existing cohesionless defects. The effective overburden, σ_v', equals σ_1' and decreases from I to III. At I, P_m is sufficient to drive the stress state into the tensile field, leading to the initiation of a pure extension fracture (black dot) perpendicular to σ_1. Note that extension fractures will only develop if the differential stress, $(\sigma_1 - \sigma_3)$, is small. At II, the least horizontal stress is reduced above and ahead of the propagating dyke, driving the stress state towards critical for fault reactivation (grey dot) or, in the absence of favourably oriented pre-existing structures, fault initiation (black dot). At III, the differential stress is very low. Because pre-existing subvertical cooling joints are ubiquitous, they are reactivated (grey dot) as a consequence of reduced horizontal stress before the differential stress is sufficient to initiate new faults. Note that the presence of favourably oriented low-cohesion normal faults precludes the reactivation of vertical structures.

pattern of dyke intrusion and associated faulting and fissuring preceded the intrusive phase of the 1975–1984 Krafla rifting episode (Einarsson 1991), leading Buck *et al.* (2006) to propose that intrusion and associated development of axial valley relief may be a typical developmental phase in the cycle of crustal accretion. Buck *et al.* (2006) argue that dyke-induced reduction of differential stress, $(\sigma_1 - \sigma_3)$, is a necessary precursor to more localized large-scale eruptive activity, though not every rifting episode will necessarily culminate in an extrusive phase. The delivery of melt to crustal levels may be sufficient to take the tectonic stress state away from that critical for fault failure but insufficient to permit extrusive activity.

To date, surface deformation and associated seismicity recorded during the Dabbahu rifting episode is consistent with dyke propagation along much of the segment, as expected on mechanical grounds during the early phase of a rifting cycle (Buck *et al.* 2006). Quantitative constraints on the temporal pattern of intrusive activity will be provided by ongoing seismic and geodetic investigations, which will inform debate on the degree of magmatic-tectonic coupling during a rifting episode. Although it remains to be seen whether the 2005 Dabbahu rifting episode will develop an extrusive phase, the similarity between recent ground breaks and the morphology of the axial zone suggests that melt delivery is sufficiently frequent that favourable stress conditions for faulting are achieved primarily during dyke events. Thus, we suggest as others have done for intermediate spreading ridges (Carbotte *et al.* 2006; Singh *et al.*

2006), that axial rift topography within the DMS reflects magma-induced deformation, rather than alternating phases of magmatism and tectonism.

7 CONCLUSIONS

Substantial fault growth occurred in tandem with magmatism (Wright *et al.* 2006; Ayele *et al.* 2007) during the 2005 Dabbahu rifting episode. Our field observations and the pattern of seismicity are largely consistent with the strain distribution induced by dyke intrusion to depths <2.5 km along the entire rift segment, as predicted from 3-D models of satellite radar data (Wright *et al.* 2006). Vertical offsets of 2-to-3 m, and horizontal offsets of <3 m, accrued on faults and associated fissures within a ∼5 km swath that extended along strike over most of the 60 km length of the segment. The locus of brittle strain was biased 5 km to the east of the rift axis in the northern half of the segment, demonstrating that dyke intrusion is not constrained to the geomorphic axis of the rift.

The amount of slip is surprisingly large given the magnitude of earthquakes recorded during the intrusive episode. The discrepancy between our observations and empirical fault scaling relationships could be explained if slip accrued incrementally over the period of dyke intrusion. Alternatively, and the subject of further

investigation, fault scaling relationships in magmatic rifts may differ from those determined for faults in a magmatic rifts.

Given the extraordinary similarity between recent ground breaks and the rift architecture in general, we suggest that fault growth in the Dabbahu Magmatic Segment predominantly occurs during periods of axial magmatism.

ACKNOWLEDGMENTS

REFERENCES

Abdallah, A. *et al*., 1979. Relevance of Afar seismicity and volcanism to the mechanics of accreting plate boundaries, *Nature,* **282,** 17–23.

Acocella, V., Korme, T. & Salvini, F., 2003. Formation of normal faults along the axial zone of the Ethiopian Rift, *J. Struct. Geol,*. **25,** 503–513.

Acton, G.D., Tessema, A., Jackson, M. & Bilham, R., 2000. The tectonic and geomagnetic significance of paleomagnetic observations from volcanic rocks from central Afar, Africa, *Earth Planet. Sci. Lett.,* **180,** 225–241.

Aki, K., 1966. Generation and propagation of G waves from the Niigata earthquake of June 16, 1964. II. Estimation of earthquake movement, release energy, and stress-strain drop from G wave spectrum, *Bull. Earthq. Res. Inst*., **44,** 23–88.

Angelier, J. & Bergerat, F., 1997. Effective tension-shear relationships in extensional fissure swarms, axial rift zone of northeastern Iceland, *J. Struct. Geol*., **19,** 673–685.

Ayele, A. *et al*., 2007. The volcano-seismic crisis in Afar, Ethiopia, starting September 2005, *Earth Planet. Sci. Lett.*, **255,** 177–187.

Barberi, F., Varet, J., 1977. Volcanism in Afar: small-scale plate tectonic implications, *Bull. Geol. Soc. Amer*., **88,** 1251–1266.

Barberi, F., Tazieff, H. & Varet, J., 1972. Volcanism in the Afar depression: its tectonic and magmatic significance, *Tectonophysics,* **15,** 19–29.

Bastow, I., Stuart, G.W., Kendall, J.-M. & Ebinger, C., 2005. Upper mantle seismic structure in a region of incipient continental breakup: northern Ethiopian rift, *Geophys. J. Int*., **162,** 479–493.

Bendick, B., McClusky, S., Bilham, R., Asfaw, L. & Klempere, S., 2006. Distributed Nubia-Somalia relative motion and dyke intrusion in the Main Ethiopian rift, *Geophys. J. Int*., **165,** 303–310.

Benoit, M.H., Nyblade, A.A., VanDecar, J.C. & Gurrola, H., 2003. Upper mantle P wave velocity structure and transition zone thickness beneath the Arabian Shield, *Geophys. Res. Lett*., **30**(10), 1531.

Benoit, M.H., Nyblade, A.A. & VanDecar, J.C., 2006. Upper mantle P wave speed variations beneath Ethiopia and the origin of the Afar Hotspot, *Geology,* **34,** 329–332.

Berckhemer, H. *et al*., 1975. Deep seismic soundings of the Afar region and on the highland of Ethiopia, in *Afar Between Continental and Oceanic Rifting,* pp. 89–107, eds Pilger, A. & Rosler, A., Schweizerbart, Stuttgart.

Bjornsson, A., Saemundsson, P., Einarsson, P., Tryggvason, E. & Gronvald, K., 1977. Current rifting episode in north Iceland, *Nature,* **266,** 318–323.

Brandsdóttir, B. & Einarsson, P., 1979. Seismic activity associated with the September 1977 deflation of Krafla volcano in North-Eastern Iceland, *J. Volcanol. Geotherm. Res.*, **6,** 197–212.

Buck, W.R., 2004. Consequences of asthenospheric variability on continental rifting, in *Rheology and Deformation of the Lithosphere at Continental Margins,* pp. 1–30, eds Karner, G.D., Taylor, B., Driscoll, N.W. & Kohlstedt, D.L., Columbia University Press, New York.

Buck, W.R., Lavier, L.L. & Poliakov, A.N.B., 2005. Modes of faulting at mid-ocean ridges, *Nature,* **434,** 719–723.

Buck, W.R., Einarsson, P. & Brandsdottir, B., 2006. Tectonic stress and magma chamber size as controls n dyke propagation: constraints from the 1975-1984 Krafla rifting episode, *J. geophys. Res.,* **111,** B12404, doi:10.1029/2005JB003879.

Cattin, R., Doubre, C., de Chabalier, J.-B., King, G., Vigny, C., Avouac, J.-P. & Ruegg, J.-C., 2005. Numerical modelling of Quaternary deformation and post-rifting displacement in the Asal-Ghoubbet rift (Djibouti, Africa), *Earth Planet. Sci. Lett.,* **239,** 352–367.

Carbotte, S.M. *et al*., 2006. Rift topography linked to magmatism at the intermediate spreading Juan de Fuca Ridge, *Geology,* **34,** 209–212.

Chadwick, Jr., W.W. & Embley, R.W., 1998. Graben formation associated with recent dyke intrusions and volcanic eruptions at the mid-ocean ridge, *J. geophys. Res.,* **103,** 9807–9825.

Chu, D. & Gordon, R.G., 1998. Current plate motions across the Red Sea, *Geophys. J. Int*., **135,** 313–328.

Clifton, A.E. & Schlische, R.W., 2003. Fracture populations on the Reykjanes Peninsula, Iceland: comparison with experimental clay models of oblique rifting, *J. geophys. Res*., **108**(B2), Art. 2074.

Clifton, A.E., Sigmundsson, F., Feigl, K.L., Gudmundsson, G. & Arnodottir, T., 2002. Surface effects of faulting and deformation resulting from magma accumulation at the Hengill triple junction, SW Iceland, 1994–1998, *J. Volc. Geothermal. Res.,* **115,** 233–255.

Cochran, J.R., 1983. A model for development of Red Sea, *Amer. Assoc. Petrol. Geol.,* **67,** 41–69.

Courtillot, V., Achache, J., Landre, F., Bonhommet, N., Montigny, R. & Feraud, G., 1984. Episodic spreading and rift propagation – new Paleomagnetic and geochronological data from the Afar nascent passive margin, *J. geophys. Res.,* **89,** 3315–3333.

Cowie, P.A., Scholz, C.H., Edwards, M. & Malinverno, A., 1993. Fault strain and seismic coupling on mid-ocean ridges, *J. geophys. Res.,* **98,** 17 911–17 920.

Curewitz, D. & Karson, J.A., 1998. Geological consequences of dyke intrusion at mid-ocean ridge spreading centers, in *Faulting and Magmatism at Mid-Ocean Ridges,* pp. 117–136, eds Buck, W.R., Delaney, P.T., Karson, J.A. & Lagabrielle, Y., Geophysical Monograph 106, AGU, Washington.

Dauteuil, O., Angelier, J., Bergerat, F., Verrier, S. & Villemin, T., 2001. Deformation partitioning inside a fissure swarm of the northern Iceland rift, *J. Struct. Geol.,* **23,** 1359–1372.

De Chabalier, J.B. & Avouac, J.P., 1994. Kinematics of the Asal rift (Djibouti) determined from the deformation of Fiele Volcano, *Science,* **265,** 1677–1681.

De Zeeuw-van Dalfsen, E., Pedersen, R., Sigmundsson, F. & Pagli, C., 2004. Satellite radar interferometry 1993–1999 suggest deep accumulation of magma near the crust-mantle boundary at the Krafla volcanic system, Iceland, *Geophys. Res. Lett.,* **31,** L13611, doi:10.1029/2004GL020059.

Dick, H.J.B., Lin, J. & Schouten, H., 2003. An ultra-slow class of ocean ridge, *Nature,* **426,** 405–411.

Dugda, M.T. & Nyblade, A.A., 2006. New constraints on crustal structure in eastern Afar from the analysis of receiver functions and surface wave dispersion in Djibouti, in *The Afar Volcanic Province within the East African Rift System,* pp. 239–251, eds Yirgu, G., Ebinger, C.J., & Maguire, P.K.H., Geological Society of London, Special Pub. 259.

Dunn, R.A., Lekic, V., Detrick, R.S. & Toome, D.R., 2005. Three-dimensional seismic structure of the Mid-Atlantic Ridge (35°N): evidence for focused melt supply and lower crustal dyke injection, *J. geophys. Res*., **110**(B9), Art. No. B09191.

Ebinger, C.J. & Casey, M., 2001. Continental breakup in magmatic provinces: an Ethiopian example, *Geology,* **29,** 527–530.

Ebinger, C., Keir, D., Ayele, A., Baker, E., Rowland, J., Wright, T. & Calais, E., 2006. Continued seismic and magmatic activity following the September 2005 rupture of the Dabbahu magmatic segment, Afar, *Eos Trans. AGU,* **87**(52), Fall Meet. Suppl., Abstract T41B-1562.

Einarsson, P., 1991. The Krafla rifting episode 1975–1989, in *Náttúra Myvatns, (The Nature of Lake Myvatn),* pp. 97–139, eds Gardarsson, A. & Einarsson, A., Icelandic Nature Science Society, Reykjavic.

Einarsson, P. & Brandsdóttir, B., 1980. Seismological evidence for lateral magma intrusion during the July 1978 deflation of the Krafla volcano in NE-Iceland, *J. geophys. Res.* **47,** 160–165.

Farr, T., & Kobrick, M., 2000. Shuttle Radar Topography Mission produces a wealth of data, *Eos Trans. AGU,* **81,** 583–585.

Feigl, K.L., Gasperi, J., Sigmundsson, F. & Rigo, A., 2000. Crustal deformation near Hengill volcano, Iceland 1993–1998: coupling between magmatic activity and faulting inferred from elastic modelling of satellite radar interferograms, *J. geophys. Res.,* **105,** 25 6552–25 670.

Foulger, G., Jahn, C., Seeber, G., Einarsson, P. Julian, B. & Heki, K., 1992. Post-rifting stress relaxation at the divergent plate boundary in northeast Iceland, *Nature,* **358,** 488–490.

Forslund, T. & Gudmundsson, A., 1991. Crustal spreading due to dykes and faults in southwest Iceland, *J. Struct. Geol.* **13,** 443–457.

Fox, C., Radford, W.E., Dziak, R., Lau, T.-K., Matsumoto, H. & Schreiner, 1995. Acoustic detection of a seafloor spreading episode on the Juan de Fuca ridge using military hydrophone arrays, *Geophys. Res. Lett.,* **22,** 131–134.

Furman, T., Bryce, J., Rooney, T., Hanan, B., Yirgu, G. & Ayalew, D., 2006. Heads and tails: 30 million years of the Afar plume, in *The Afar Volcanic Province within the East African Rift System,* pp. 95–119, eds Yirgu, G., Ebinger, C.J. & Maguire, P.K.H., Geological Society of London, Special Pub. 259.

Grant, J.V. & Kattenhorn, S.A., 2004. Evolution of vertical faults at an extensional plate boundary, southwest Iceland, *J. Struct. Geol.* **26,** 537–557.

Gudmundsson, A., 1992. Formation and growth of normal faults at the divergent palte boundary in Iceland, *Terra Nova,* **4,** 464–471.

Gupta, A. & Scholz, C.H., 2000. Brittle strain regime transition in the Afar depression: implications for fault growth and seafloor spreading, *Geology,* **28,** 1087–1090.

Hanks, T.C. & Kanamori, H., 1979. A moment-magnitude scale, *J. geophys. Res.,* **84,** 2348–2350.

Hayward, N.J., 1997. A quantitative comparison of oceanic and continental rift segmentation. Unpubl. *PhD thesis,* University of Leeds, United Kingdom.

Hayward, N.J. & Ebinger, C.J., 1996. Variations in the along-axis segmentation of the Afar Rift system. *Tectonic*s, **15,** 244–257.

Heki, K., Foulger, G.R., Julian, B.R. & Jahn, C.-H., 1993. Plate kinematics near divergent boundaries: geophysical implications of post-tectonic crustal deformation in NE Iceland detected using the Global Positioning System, *J. geophys. Res.* **98,** 14 279–14 297.

Hofman, C., Courtillot, V., Feraud, G., Rochette, P., Yirgu, G., Ketefo, E. & Pik, R., 1997. Timing of the Ethiopian flodd basalt event and implications for plume birth and global change, *Nature,* **389**(6653), 838–841.

Hofstetter, R., & Beyth, M., 2003. The Afar Depression: interpretation of the 1960–2000 earthquakes, *Geophys. J. Int.,* **155,** 715–732.

Holland, M., Urai, J.L. & Martel, S., 2006. The internal structure of fault zones in basaltic sequences, *Earth Planet. Sci. Lett.,* **248,** 301–315.

Jacques, E., Ruegg, J.C., Lepine, J.C., Tapponnier, P., King, G.C.P. & Omar, A., 1999. Relocations of M ≥2 events of the 1989 Dobi seismic sequence in Afar: evidence for earthquake migration, *Geophys. J. Int.,* **138,** 447–469.

Jestin, F., Huchon, P. & Gaulier, J.M., 1994. The Somalia plate and the East African Rift System: present-day kinematics, *Geophys. J. Int.,* **116,** 637–654.

Keir, D., Kendall, J.M., Ebinger, C.J. & Stuart, G.W., 2005. Variations in late syn-rift melt alignment inferred from shear-wave splitting in crustal earthquakes beneath the Ethiopian Rift, *Geophys. Res. Lett.,* **32,** Art. No. L23308.

Keir, D., Ebinger, C.J., Stuart, G.W., Daly, E. & Ayele, A., 2006a. Strain accommodation by magmatism and faulting at continental breakup: seismicity of the northern Ethiopian rift, *J. geophys. Res.,* **111,** doi:10.1029/2005JB003748.

Keir, D., Wright, T., Ebinger, C., Ayele, A., Bellachew, M., Calais, E. & Lewi, E., 2006b. June 2006 dyke intrusion in the Dabbahu magmatic segment, Afar, Ethiopia, *Eos Trans. AGU,* **87**(52), Fall Meet. Suppl. Abstract, T33E-05.

Kendall, J.-M., Stuart, G., Ebinger, C., Bastow, I. & Keir, D., 2005. Magma-assisted rifting in Ethiopia, *Nature,* **433,** 146–148.

Kent, G.M. *et al.*, 2000. Evidence from three-dimensional seismic reflectivity images for enhanced melt supply beneath mid-ocean-ridge discontinuities, *Nature,* **406,** 614–618.

Keranen, K., Klempere, S., Gloaguen, R. & EAGLE Working Group, 2004. Three-dimensional seismic imaging a proto-ridge axis in the Main Ethiopian Rift, *Geology,* **32,** 949–952.

Kidane, T. *et al.*, 2003. New Paleomagnetic and geochronological results from Ethiopian Afar: block rotations linked to rift overlap and propagation and determination of a similar to 2 Ma reference pole for stable Africa, *J. geophys. Res.*, **108,** doi:2102:00018198520001.

Klausen, M.B. & Larsen, H.C., 2002. East Greenland coast-parallel dyke swarm and its role in continental breakup, in *Volcanic Rifted Margins, Geol. Soc. Amer. Spec. Pub.*, Vol. 362, pp. 133–158, eds Menzies, M., Klemperer, S., Ebinger, C., Baker, J., Geological Society of America, Boulder.

Lahitte, P., Gillot, P.-Y. & Courtillot, V., 2003. Silicic central volcanoes as precursors to rift propagation: the Afar case, *Earth Planet. Sci. Lett.*, **207,** 103–116.

Langmuir, C.H., Bender, J.F. & Batiza, R., 1986. Petrological and tectonic segmentation of the East Pacific Rise, 5°30′–14°30′ N, *Nature,* **322,** 422–429.

Lin, J. & Phipps Morgan, J., 1992. The spreading rate dependence of three-dimensional mid-ocean ridge gravity structure, *Geophys. Res. Lett.*, **19,** 13–16.

Lister, J.R. & Kerr, R.C., 1991. Fluid-mechanical models of crack propagation and their application to magma transport in dykes, *J. geophys. Res.*, **96,** 10 049–10 077.

McClay, K.R., Dooley, T., Whitehouse, P. & Mills, M., 2002. 4-D evolution of rift systems: insights from scaled physical models, *AAPG Bull.*, **86,** 935–959.

Macdonald, K.C. *et al.*, 1988. A new view of the mid-ocean ridge from the behaviour of ridge-axis discontinuities, *Nature,* **335,** 217–225.

Mackenzie, G.D., Thybo, H. & Maguire, P.K.H., 2005. Crustal velocity structure across the Main Ethiopian Rift: results from two-dimensional wide-angle seismic modelling, *Geophys. J. Int.*, **162,** 994–1006.

Manighetti, I., Tapponier, P., Gillot, P.Y., Jacques, E., Courtillot, V., Armijo, R., Ruegg, J.C. & King, G., 1998. Propagation of rifting along the Arabia-Somalia plate boundary: into Afar, *J. geophys. Res.*, **103,** 4947–4974.

Manighetti, I., King, G.C.P., Gaudemer, Y., Scholz, C.H. & Doubre, C., 2001. Slip accumulation and lateral propagation of active normal faults in Afar, *J. geophys. Res.*, **106,** 13 667–13 696.

Martel, S.J. & Langley, J.S., 2006. Propagation of normal faults to the surface in basalt, Koae fault system, Hawaii, *J. Struct. Geol.,* **28,** 2123–2143.

Mohammadioun, B. & Serva, L., 2001. Stress drop, slip type, earthquake magnitude, and seismic hazard, *Bull. Seism. Soc. Am.*, **91,** 694–707.

Montelli, R., Nolet, G., Dahlen, F.A., Masters, G., Engdahl, E.R. & Hung, S.-H., 2004. Finite-frequency tomography reveals a variety of plumes in the mantle, *Science,* **303,** 338–343.

Muffler, P., Clynne, M. & Champion, D., 1994. Late Quaternary normal faulting of the Hat Creek Basalt, northern California, *Bull. Geol. Soc. Am.*, **106,** 195–200.

Oppenheimer, C. & Francis, P., 1997. Remote sensing of heat, lava and fume-role emissions from Erta'Ale volcano, Ethiopia, *Int. J. Remote Sensing,* **18,** 1661–1692.

Parsons, T., Thompson, G.A. & Smith, R.P., 1998. More than one way to stretch: a tectonic model for extension along the plume trail of the Yellowstone hotspot and adjacent basin and Range Province, *Tectonics,* **17,** 221–234.

Peacock, D.C.P. & Parfit, E.A., 2002. Active relay ramps and normal fault propagation on Kilauea Volcano, Hawaii, *J. Struct. Geol.*, **24,** 729–742.

Peirce, C., Gardiner, A. & Shaw, M., 2005. Temporal and spatial cyclicity of accretion at slow-spreading ridges – evidence from Reykjanes Ridge, *Geophys. J. Int.*, **163,** 56–78.

Pollard, D.D. & Aydin, A., 1984. Propagation and linkage of oceanic ridge segments, *J. geophys. Res.,* **89,** 10 017–10 028.

Pollard, D.D., Segall, P. & Delaney, P.T., 1982. Formation and interpretation of dilatent echelon cracks, *Bull. Geol. Soc. Amer.,* **93,** 1291–1303.

Pollard, D.D., Delaney, P.T., Duffield, W.A., Endo, E.T. & Okamura, A.T., 1983. Surface deformation in volcanic rift zones, *Tectonophysics,* **94,** 541–584.

Qin, R., Buck, W.R., Calais, E. & Wright, T., 2006. Effects of viscoelastic relaxation and continuing dyke intrusions on surface deformation during 2005 Afar diking episode, *Eos Trans. AGU,* **87** (52), Fall Meet. Suppl. Abstract, T41B-1565.

Rubin, A.M., 1992. Dyke-induced faulting and graben subsidence in volcanic rift zones, *J. geophys. Res.,* **97,** 1839–1858.

Rubin, A.M. & Pollard, D.D., 1987. Origins of blade-like dykes in volcanic rift zones, Vol. 1350, pp. 1449–1470, in *Volcanism in Hawaii,* eds Decker, R.W., Wright, T.L. & Stauffer, P., USGS Prof. Paper.

Rubin, A.M. & Pollard, D.D., 1988. Dyke-induced faulting in rift zones of Iceland and Afar, *Geology,* **16,** 413–417.

Schilling, J.-G., Kingsley, R., Hanan, B. & McCully, B., 1992. Nd-Sr-Os isotopic variations along the Gulf of Aden: evidence for mantle-plume lithosphere interaction., *J. geophys. Res.,* **97,** 10 927–10 966.

Sempéré, J.-C., Lin, J., Brown, H.S., Schouten, H. & Purdy, G.M., 1993. Segmentation and morphotectonic variations along a slow-spreading center: the Mid-Atlantic Ridge (24°00′ N-30°40′ N), *Mar. geophys. Res.,* **15,** 153–200.

Sigmundsson, F., 2006. *Iceland Geodynamics: Crustal Deformation and Divergent Plate Tectonics,* Springer-Praxis, 228 p.

Singh, S.C. *et al.,* 2006. Discovery of a magma chamber and faults beneath a Mid-Atlantic Ridge hydrothermal field, *Nature,* **442,** 1029–1032.

Smith, R.P., Jackson, S.M. & Hackett, W.R., 1996. Paleoseismology and seismic hazards evaluation in extensional volcanic terrains, *J. geophy. Res.,* **101,** 6277–6292.

Stuart, G.W., Bastow, I.D. & Ebinger, C.J., 2006. Crustal structure of the northern Main Ethiopian Rift from receiver function studies, in *The Afar Volcanic Province within the East African Rift System,* pp. 253–267, eds Yirgu, G., Ebinger, C.J., & Maguire, P.K.H., Geological Society of London, Special Pub. 259.

Tapponnier, P., Armijo, R., Manighetti, I. & Courtillot, V., 1990. Bookshelf faulting and horizontal block rotations between overlapping rifts in southern Afar, *Geophys. Res. Lett.,* **17,** 1–4.

Tentler, T., 2005. Propagation of brittle failure triggered by magma in Iceland, *Tectonophysics,* **406,** 17–38.

Thatcher, W. & Hill, D.P., 1995. A simple model for fault generated morphology of slow-spreading mid-ocean ridges, *J. geophys. Res.,* **100,** 561–570.

Tiberi, C., Ebinger, C., Ballu, V., Stuart, G. & oluma, B., 2005. Inverse models of gravity data from the Red Sea – Aden – East African Rift triple junction zone, *Geophys. J. Int.,* **163,** 775–787.

Tucholke, B.E. & Lin, J., 1994. A geological model for the structure of ridge segments in slow spreading ocean crust, *J. geophys. Res.,* **99,** 11 937–11 958.

Van Adendonk, H.J.A., Harding, A.J., Orcutt, J.A. & McClain, J.S., 2001. Contrast in crustal structure across the Clipperton transform fault from travel time tomography, *J. geophys. Res.,* **106,** 10 961–10 981.

Van Wyk de Vries, B. & Merle, O., 1996. The effect of volcano constructs on rift fault patterns, *Geology,* **24,** 643–646.

Vigny, C., Huchon, P., Ruegg, J.-C., Khanbari, K. & Asfaw, L.M., 2006. Confirmation of Arabia slow motion by new GPS data in Yemen, *J. geophys. Res.,* **111,** B02402, doi:10.1029/2004JB003229.

Wells, D.L. & Coppersmith, K.J., 1994. New empirical relationships among magnitude, rupture length, rupture width, rupture area, and surface displacement, *Bull. Seis. Soc. Amer.,* **84,** 974–1002.

Wolfenden, E., Ebinger, C., Yirgu, G., Renne, P. & Kelley, S.P., 2005. Evolution of the southern Red Sea rift: birth of a magmatic margin, *Bull. Geol. Soc. Amer.,* **117,** 846–864.

Wright, T., Ebinger, C.J., Biggs, J., Ayele, A., Yirgu, Keir, D. & Stork, A., 2006. Magma-maintained rift segmentation at continental rupture in the 2005 Afar dyking episode, *Nature,* **422,** 291–294.

Yirgu, G., Ayele, A. & Ayalew, D., 2006. Recent seismovolcanic crisis in Northern Afar, Ethiopia, *Eos,* **87(** 33), 325–336.